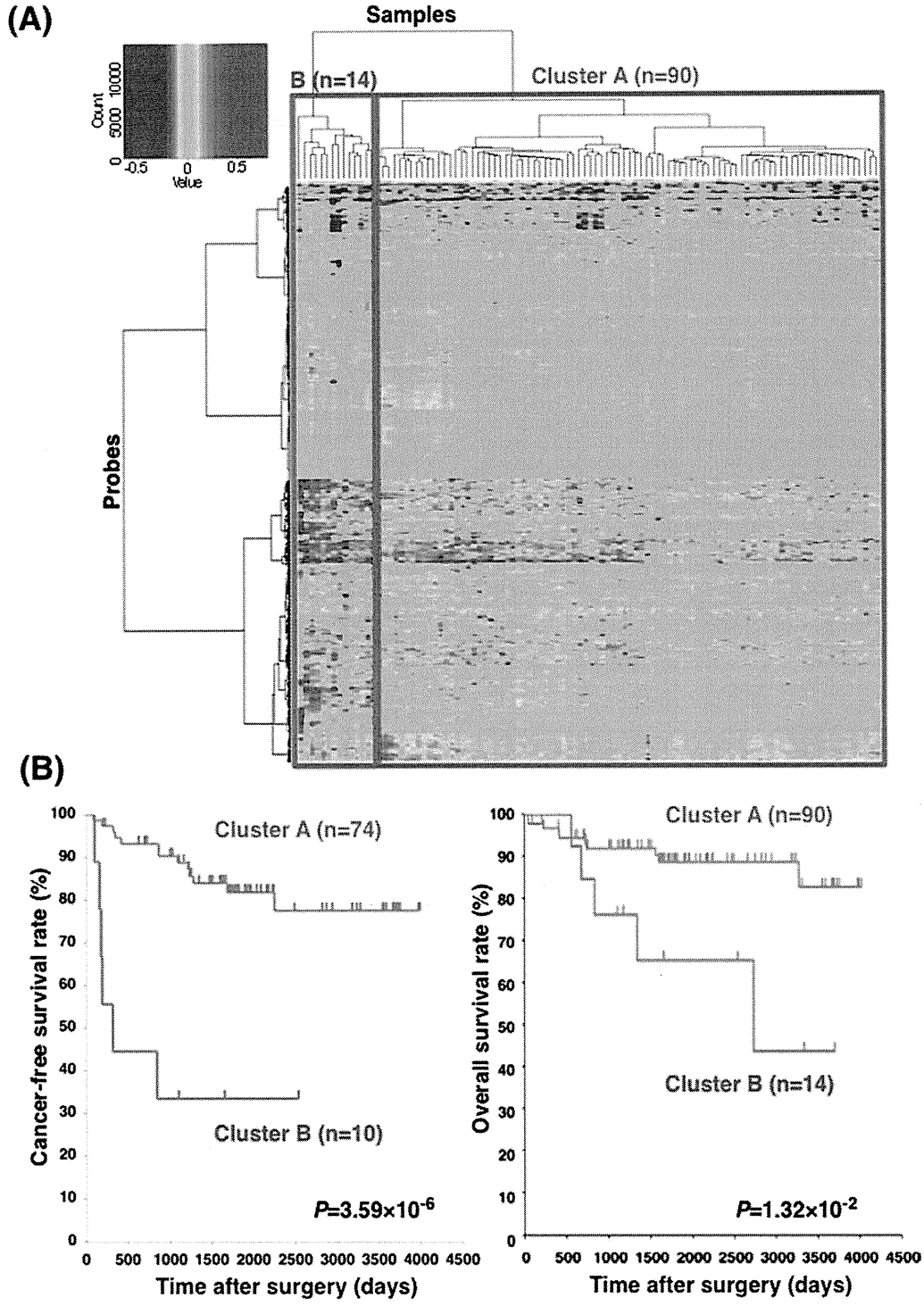

Fig. 1. Unsupervised hierarchical clustering using DNA methylation levels ($\Delta\beta_{T-N}$) on the 801 probes in 104 patients with clear cell RCCs. The 801 probes satisfied all of the criteria (a), (b) and (c) in 'DNA methylation alterations during renal carcinogenesis' in Results and Table I. On the 801 probes, DNA methylation alterations occurred at the precancerous stages and were inherited by and strengthened in clear cell RCCs themselves. (**A**) 104 patients with clear cell RCCs were hierarchically clustered into Cluster A (n = 90) and Cluster B (n = 14). The DNA methylation levels ($\Delta\beta_{T-N}$) are shown in the color range maps. The cluster trees for patients and probes are shown at the top and left of the panel, respectively. (**B**) The cancer-free ($P = 3.59 \times 10^{-6}$) survival rates of Stage I–III patients in Cluster B were significantly lower (log-rank test) than those of patients in Cluster A. Overall ($P = 1.32 \times 10^{-2}$) survival rates of all patients in Cluster B were significantly lower (log-rank test) than those of patients in Cluster A.

Epigenetic clustering of clear cell RCCs

Unsupervised hierarchical clustering using DNA methylation levels ($\Delta\beta_{T-N}$) on the above 801 probes, on which DNA methylation alterations occurred at the precancerous stages and may continuously participate in renal carcinogenesis, subclustered 104 patients with clear cell RCCs, of whom both N and T samples were assayed in the same experimental batch, into Cluster A (n = 90) and Cluster B (n = 14, Figure 1A). The clinicopathological parameters of clear cell RCCs belonging to Clusters A and B are summarized in Table II. (The number of samples for each TNM stage is also described in Supplementary Table S3, available at *Carcinogenesis* Online.) Epigenetic clustering of clear cell RCCs was dependent on neither age nor sex of the patients (Table II). Clear cell RCCs belonging to Cluster B had a larger diameter, more frequent macroscopically evident extranodular (type 2) or multinodular (type 3) growth, vascular involvement, renal vein tumor thrombi, infiltrating growth, tumor necrosis and renal pelvis invasion, and also had higher histological grades and pathological TNM stages than those in Cluster A (Table II). Figure 1B shows the Kaplan–Meier survival curves of patients belonging to Clusters A and B. The period covered ranged from 42 to 4024 days (mean, 1821 days). The cancer-free and overall survival rates of patients in Cluster B were significantly lower than those of patients in Cluster A ($P = 3.59 \times 10^{-6}$ and $P = 1.32 \times 10^{-2}$, respectively, Figure 1B).

Table II. Correlation between the subclassification of patients with clear cell RRCs based on DNA methylation profiles and the clinicopathological parameters

Clinicopathological parameters		Cluster A (n = 90)	Cluster B (n = 14)	P [a]
Age		62.08 ± 10.08	67.36 ± 11.06	8.36×10^{-2} [b]
Sex	Male	63	11	5.47×10^{-1} [c]
	Female	27	3	
Tumor diameter (cm)		5.10 ± 3.19	8.75 ± 2.85	*1.07×10^{-4}* [b]
Macroscopic configuration	Type 1	37	1	*6.29×10^{-4}* [c]
	Type 2	29	2	
	Type 3	24	11	
Predominant histological grades[d]	G1	47	1	*8.33×10^{-6}* [c]
	G2	35	4	
	G3	7	7	
	G4	1	2	
Highest histological grades[e]	G1	8	0	*5.67×10^{-4}* [c]
	G2	43	1	
	G3	24	4	
	G4	15	9	
Vascular involvement	Negative	54	1	*2.45×10^{-4}* [c]
	Positive	36	13	
Renal vein tumor thrombi	Negative	69	5	*3.38×10^{-3}* [c]
	Positive	21	9	
Predominant growth pattern[d]	Expansive	84	7	*1.86×10^{-4}* [c]
	Infiltrative	6	7	
Most aggressive growth pattern[e]	Expansive	57	4	*2.06×10^{-3}* [c]
	Infiltrative	33	10	
Tumor necrosis	Negative	71	2	*4.86×10^{-6}* [c]
	Positive	19	12	
Invasion to renal pelvis	Negative	83	10	*3.98×10^{-2}* [c]
	Positive	7	4	
Pathological TNM stage	Stage I	50	0	*5.41×10^{-5}* [c]
	Stage II	1	1	
	Stage III	23	9	
	Stage IV	16	4	

The number of samples in each TNM stage was described in Supplementary Table S3, available at *Carcinogenesis* Online.
[a]*P*-values of <0.05 are in italics.
[b]Wilcoxon rank sum test.
[c]Fisher's exact test.
[d]If the tumor showed heterogeneity, findings in the predominant area were described.
[e]If the tumor showed heterogeneity, the most aggressive features of the tumor were described.

DNA methylation profiles of clear cell RCCs belonging to each cluster

The distribution of DNA methylation levels ($\Delta\beta_{T-N}$) in all 26 454 probes for 104 clear cell RCCs belonging to Cluster A or B is summarized along chromosomes in Figure 2A. Clear cell RCCs belonging to Cluster B clearly showed accumulation of DNA hypermethylation ($\Delta\beta_{T-N} > 0.1$) relative to DNA hypomethylation, whereas clear cell RCCs belonging to Cluster A showed greater DNA hypomethylation ($\Delta\beta_{T-N} < -0.1$) relative to DNA hypermethylation (Figure 2A).

The proportions of the probes showing the various degrees of DNA hypermethylation in T samples compared with the corresponding N samples ($\Delta\beta_{T-N} > 0.1$, 0.2, 0.3, 0.4 or 0.5) for all 26 454 probes, and the proportions of the probes showing various degrees of DNA hypomethylation in T samples compared with the corresponding N samples ($\Delta\beta_{T-N} < -0.1$, −0.2, −0.3, −0.4 or −0.5) for all 26 454 probes in clear cell RCCs belonging to Clusters A and B are summarized in Figure 2B. Although the probes showing prominent DNA hypomethylation ($\Delta\beta_{T-N} < -0.5$) were accumulated slightly more in Cluster B than in Cluster A, the incidence of DNA hypomethylation in Clusters A and B did not reach a statistically significant difference ($\Delta\beta_{T-N} < -0.1$, −0.2, −0.3 or −0.4, Figure 2B). On the other hand, the probes showing DNA hypermethylation were markedly accumulated in Cluster B relative to Cluster A, regardless of the degree of DNA hypermethylation ($\Delta\beta_{T-N} > 0.1$, 0.2, 0.3, 0.4 or 0.5, Figure 2B). These data indicate that clear cell RCCs belonging to Cluster B are characterized by accumulation of DNA hypermethylation.

The top 61 probes (including the 60th and 61st, which showed equivalent P-values) on which DNA methylation levels ($\Delta\beta_{T-N}$) differed markedly between Clusters A and B ($P < 1.056 \times 10^{-6}$, Wilcoxon rank sum test) are listed in Supplementary Table S4, available at *Carcinogenesis* Online. Although only 19 246 probes (72.8%) out of the total of 26 454 were located within CpG islands, 60 (98.4%) of the top 61 probes located within CpG islands showed DNA hypermethylation in clear cell RCCs belonging to Cluster B ($\Delta\beta_{T-N} > 0.097$, Supplementary Table S4, available at *Carcinogenesis* Online): only 1 probe among the top 61 was located within a non-CpG island and showed DNA hypomethylation ($\Delta\beta_{T-N} = -0.425 \pm 0.096$ in Cluster B). Taken together, the data indicated that Cluster B is significantly correlated with clinicopathological phenotype and characterized by frequent DNA hypermethylation on CpG islands. Such characteristics of clear cell RCCs in Cluster B are similar to those of CpG island methylator phenotype (CIMP)-positive cancers (30,31) in other well-studied organs, such as those of the colon (32) and stomach (33). In other words, our single-CpG-resolution methylome analysis identified, for the first time, CIMP-positive clear cell RCCs as Cluster B.

Hallmark CpG sites of CIMP-positive clear cell RCCs

Scattergrams of DNA methylation levels (β values) in T and the corresponding N samples from representative patients with clear cell RCCs belonging to Clusters A and B (Supplementary Figure S3, available at *Carcinogenesis* Online) indicated that probes for which DNA methylation levels were low in the N samples and for which the degree of DNA hypermethylation in T samples relative to the corresponding N samples was prominent (marked by red circles in panels E to H in Supplementary Figure S3, available at *Carcinogenesis* Online) were obvious only in Cluster B, and not in Cluster A.

Therefore, in order to discriminate clear cell RCCs belonging to Cluster B from those belonging to Cluster A, we first focused on the probes for which the average β value in all N samples was less than 0.2 and the incidence of more than $0.4\Delta\beta_{T-N}$ was markedly higher in Cluster B relative to Cluster A ($P < 1.98 \times 10^{-6}$, Fisher's exact test). Among such probes, 16 (the FAM150A, GRM6, ZNF540, ZFP42, ZNF154, RIMS4, PCDHAC1, KHDRBS2, ASCL2, KCNQ1, PRAC, ZNF154, WNT3A, TRH, FAM78A and ZNF671 genes) showed $>0.4\Delta\beta_{T-N}$ in 6 (42.8%) or more RCCs among the 14 belonging to Cluster B, but only in 2 (2.2%) or fewer RCCs among the 90 belonging to Cluster A (Table IIIA). DNA methylation levels ($\Delta\beta_{T-N}$) on the 16 CpG sites differed completely between Clusters A and B (Supplementary Figure S4, available at *Carcinogenesis* Online). In addition,

random forest analysis (27) (Supplementary Figure S5, available at *Carcinogenesis* Online) using the 869 probes on which DNA methylation levels ($\Delta\beta_{T-N}$) differed significantly between Clusters A and B [FDR (q = 0.01)] identified the top four probes that were able to discriminate Cluster B from Cluster A in Table IIIB. Two probes were shared by Tables IIIA and IIIB. Thus, CpG sites on the 18 probes can be considered as hallmarks of CIMP-positive clear cell RCCs, i.e. clear cell RCCs belonging to Cluster B.

Discussion

Here, we have reported the results of methylome analysis of 245 renal tissue samples at single-CpG resolution. To our knowledge, no study involving Infinium analysis of such a large number of renal tissue samples has been reported to date. We have been focusing on DNA methylation alterations at the precancerous stage: our previous studies using methylation-specific PCR, combined bisulfite restriction enzyme analysis and bacterial artificial chromosome arrays suggested that N samples are already at the precancerous stage associated with DNA methylation alterations (17–20). First, we identified the probes on which DNA methylation status in N samples were significantly altered relative to those in C samples. The single-CpG-resolution analysis revealed that the DNA methylation status of 4830 CpG sites was actually altered at the precancerous stage in comparison to normal renal cortex tissue samples. In addition, it was revealed that alterations at the precancerous stages tended to involve DNA hypermethylation [Table I(a)]. Among the 801 probes we selected, DNA methylation alterations occurred at the precancerous stage and were inherited by, and strengthened in, clear cell RCCs themselves, indicating that DNA methylation alterations on the 801 probes may participate continuously in renal carcinogenesis from the precancerous stage until cancers have become established. The DNA methylation profiles of these 801 probes clustered clear cell RCCs into clinicopathologically valid subclusters: clear cell RCCs belonging to Cluster B showed clinicopathological parameters reflecting tumor aggressiveness, and patients with Cluster B tumors showed a poorer outcome. Quantitative reverse transcription–PCR analysis indicated that DNA hypermethylation may result in significantly reduced expression of representative genes listed in Tables IIIA and IIIB and Supplementary Table S4, available at *Carcinogenesis* Online (Supplementary Table S5, available at *Carcinogenesis* Online). These findings suggest that DNA

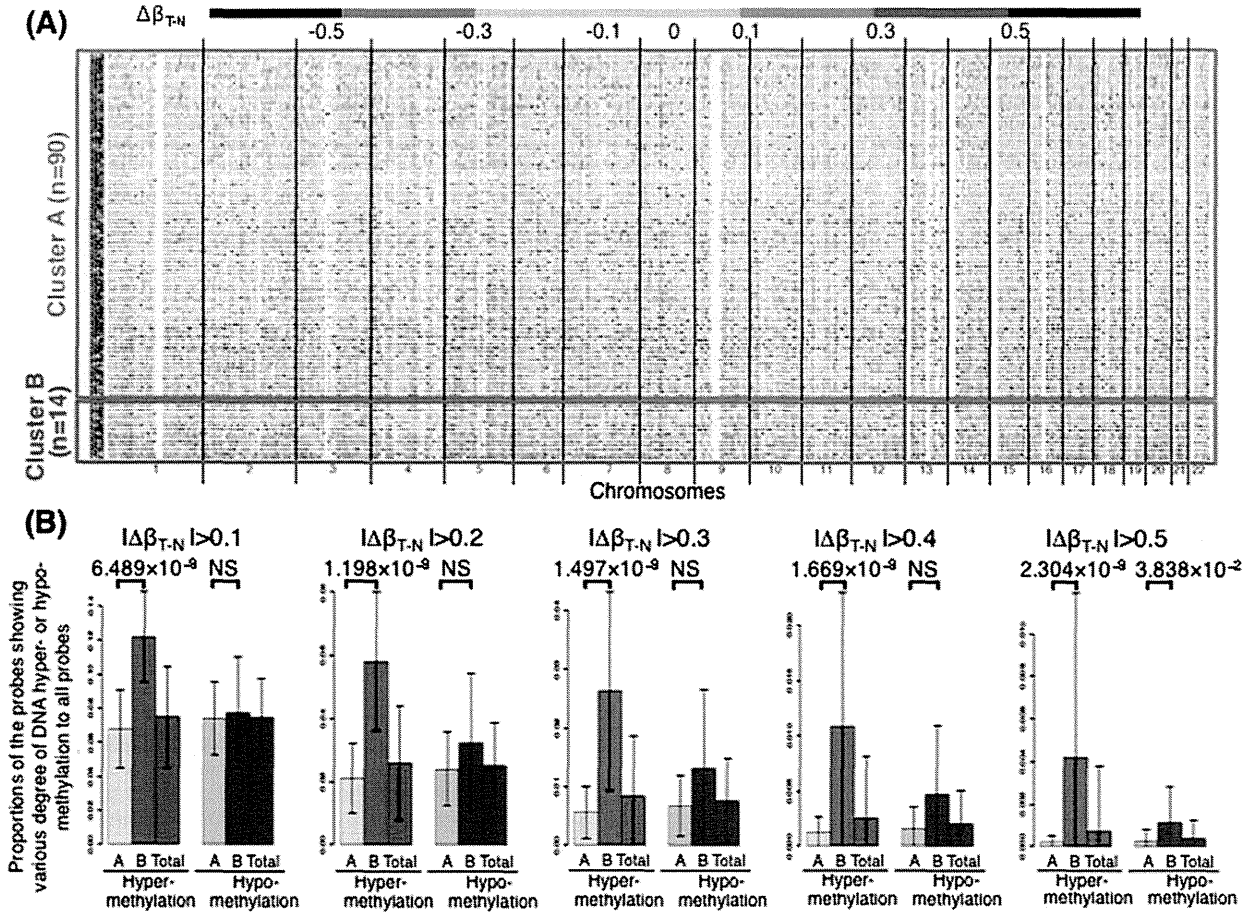

Fig. 2. (**A**) Distribution of DNA methylation levels ($\Delta\beta_{T-N}$) in all 26 454 probes in 104 clear cell RCCs belonging to Cluster A or B. The DNA methylation levels are shown in the color range maps. Clear cell RCCs belonging to Cluster A are skewed toward DNA hypomethylation ($\Delta\beta_{T-N} < -0.1$, cold color) relative to DNA hypermethylation (warm color). Clear cell RCCs belonging to Cluster B clearly showed accumulation of DNA hypermethylation ($\Delta\beta_{T-N} > 0.1$, warm color) relative to DNA hypomethylation (cold color). (**B**) The proportions of the probes showing the various degrees of DNA hypermethylation, when the tumor tissue (T) sample was compared with the corresponding non-cancerous renal cortex tissue (N) sample ($\Delta\beta_{T-N} > 0.1$, 0.2, 0.3, 0.4 or 0.5, warm color), to all probes, and the proportions of the probes showing the various degrees of DNA hypomethylation, when the T sample was compared with the corresponding N sample ($\Delta\beta_{T-N} < -0.1$, −0.2, −0.3, −0.4 or −0.5, cold color), to all probes in Clusters A and B. Bar, standard deviation. The probes showing DNA hypermethylation were markedly accumulated in Cluster B relative to Cluster A, regardless of the degree of DNA hypermethylation ($\Delta\beta_{T-N} > 0.1$, 0.2, 0.3, 0.4 or 0.5). The probes showing prominent DNA hypomethylation ($\Delta\beta_{T-N} < -0.5$) were slightly accumulated in Cluster B compared with Cluster A. These data indicated that clear cell RCCs belonging to Cluster B are mainly characterized by accumulation of DNA hypermethylation.

Table IIIA. CpG sites as hallmarks of the CpG island methylator phenotype of clear cell RRCs

Target ID[a]	Chr[b]	Position[c]	CpG island[d]	Gene symbol	The number of tumors whose $\Delta\beta_{T-N} > 0.4$ (%)[e]		P[f]
					Cluster A ($n = 90$)	Cluster B ($n = 14$)	
cg17162024	8	53,478,454	Y	FAM150A	2 (2.2)	12 (85.7)	4.60×10^{-12}
cg14859460	5	178,422,244	Y	GRM6	0 (0)	10 (71.4)	3.84×10^{-11}
cg03975694	19	38,042,472	Y	ZNF540	2 (2.2)	9 (64.3)	3.64×10^{-8}
cg06274159	4	188,916,867	Y	ZFP42	1 (1.1)	8 (57.1)	9.91×10^{-8}
cg08668790	19	58,220,662	Y	ZNF154	1 (1.1)	8 (57.1)	9.91×10^{-8}
cg19332710	20	43,438,865	Y	RIMS4	2 (2.2)	8 (57.1)	4.68×10^{-7}
cg12629325	5	140,306,458	Y	PCDHAC1	2 (2.2)	7 (50)	5.10×10^{-6}
cg18239753	6	62,995,963	Y	KHDRBS2	2 (2.2)	7 (50)	5.10×10^{-6}
cg06263495	11	2,292,004	Y	ASCL2	2 (2.2)	7 (50)	5.10×10^{-6}
cg17575811	11	2,466,409	Y	KCNQ1	1 (1.1)	7 (50)	1.21×10^{-6}
cg12374721	17	46,799,640	Y	PRAC	2 (2.2)	7 (50)	5.10×10^{-6}
cg21790626	19	58,220,494	Y	ZNF154	0 (0)	7 (50)	1.62×10^{-7}
cg01322134	1	228,194,448	Y	WNT3A	0 (0)	6 (42.9)	1.98×10^{-6}
cg01009664	3	129,693,613	Y	TRH	0 (0)	6 (42.9)	1.98×10^{-6}
cg12998491	9	134,152,531	Y	FAM78A	0 (0)	6 (42.9)	1.98×10^{-6}
cg19246110	19	58,238,928	Y	ZNF671	0 (0)	6 (42.9)	1.98×10^{-6}

[a]Probe ID for the Infinium HumanMethylation27 Bead Array.
[b]Chromosome.
[c]National Center for Biotechnology Information (NCBI) Database (Genome Build 37).
[d]Y means CpG island.
The probes satisfied the following criteria: (i) the average β value for all samples of non-cancerous renal cortex tissue (N) was <0.2, (ii) $>0.4\Delta\beta_{T-N}$ was observed in six or more clear cell RCCs (≥42.9%)[e] in Cluster B, whereas $>0.4\Delta\beta_{T-N}$ in two or fewer clear cell RCCs (≤2.2%)[e] in Cluster A and (iii) the incidence of $>0.4\Delta\beta_{T-N}$ was markedly higher in Cluster B than in Cluster A ($P < 1.98 \times 10^{-6}$, Fisher's exact test[f]).

Table IIIB. CpG sites as hallmarks of the CpG island methylator phenotype of clear cell RRCs

Target ID[a]	Chr[b]	Position[c]	CpG island[d]	Gene symbol	$\Delta\beta_{T-N}$ (mean ± SD)		P[e]
					Cluster A ($n = 90$)	Cluster B ($n = 14$)	
cg17162024	8	53,478,454	Y	FAM150A[f]	0.126±0.120	0.499±0.184	3.40×10^{-7}
cg22040627	17	6,617,030	Y	SLC13A5	0.045±0.072	0.283±0.103	2.64×10^{-7}
cg14859460	5	178,422,244	Y	GRM6[f]	0.077±0.105	0.434±0.184	1.10×10^{-7}
cg09260089	10	134,599,860	Y	NKX6-2	0.078±0.083	0.372±0.150	2.26×10^{-7}

[a]Probe ID of the Infinium HumanMethylation27 Bead Array.
[b]Chromosome.
[c]NCBI Database (Genome Build 37).
[d]Y means CpG island.
[e]Top four probes capable of discriminating Cluster B from Cluster A identified by random forest analysis (Supplementary Figure S5, available at *Carcinogenesis* Online) using the 869 probes on which the DNA methylation levels ($\Delta\beta_{T-N}$) were differed significantly between Clusters A and B (Wilcoxon rank sum test).
[f]The FAM150A and GRM6 genes were shared by Tables IIIA and IIIB.

methylation alterations occurring at the precancerous stage determine both the aggressiveness of RCCs and the outcome of affected patients through alterations of gene expression levels.

Unsupervised hierarchical clustering based on our previous study using bacterial artificial chromosome arrays also clustered clear cell RCCs into clinicopathologically valid subclusters: 14% of examined RCCs belonged to a subcluster showing clinicopathological parameters reflecting tumor aggressiveness and poorer patient outcome (19). DNA methylation profiles in N samples based on BAMCA data were also inherited by the corresponding clear cell RCC developing in the same patient. In this study, 14% of the clear cell RCCs subjected to Infinium analysis belonged to Cluster B. BAMCA is suitable for detecting DNA methylation alterations occurring in a coordinated manner on individual large regions of chromosomes (34–37), whereas 27 000 Infinium array is suitable for detecting DNA methylation alterations on promoter regions of specific genes. Different methodologies identified similar clinicopathologically valid subclusters of RCCs, indicating that such clustering based on DNA methylation profiles is not accidental but reproducible, and may reflect the distinct epigenetic pathway of renal carcinogenesis.

In contrast to Cluster A, which appeared to be characterized by accumulation of DNA hypomethylation (Figure 2A), Cluster B was clearly characterized by accumulations of DNA hypermethylation on CpG islands. Since Cluster B was significantly associated with both frequent DNA hypermethylation on CpG islands and distinct clinicopathological phenotypes of clear cell RCCs, RCCs belonging to Cluster B can be recognized as CIMP-positive clear cell RCCs on the basis of the definition of well-studied CIMP-positive cancers (30,31) such as colorectal cancer (32) and stomach cancer (33), although Morris *et al.* (28) previously considered that the relevance of the CIMP-positive phenotype to RCCs had not yet been clearly defined. Although McRonald *et al.* (29) suggested that a subset of RCCs might display CIMP based on findings indicating that the distribution of the number of methylated CpGs in individual tumors differed from the expected Poisson distribution, they did not identify distinct CpG sites that could become hallmarks for CIMP in the kidney. It has been suggested that, in order to identify CIMP-positive cancers in specific organs, marker CpG sites or genes that are specific to each organ or histological type of tumor should be used (38), rather than classical CIMP marker genes (30,31) that were originally identified in colorectal cancers. The present single-CpG-resolution analysis identified such hallmark CpG sites for the first time. Using the 18 CpG sites in Tables IIIA and IIIB, CIMP-positive RCCs or RCCs equivalent to those in the present Cluster B could be reproducibly identified. These 18 CpG sites may be useful for further clarifying the molecular basis of the epigenetic pathway of renal carcinogenesis.

DNA methylation alterations are known to result in chromosomal instability through chromatin configuration changes (39). In fact, germline mutations of the de novo DNA methyltransferase DNMT3B gene have been reported in patients with immunodeficiency, centromeric instability and facial anomalies (ICF) syndrome, a rare recessive autosomal disorder characterized by DNA hypomethylation of pericentromeric satellite regions (40). In HCCs and urothelial carcinomas, DNA hypomethylation of these regions is correlated with copy number alterations on chromosomes 1 (41) and 9 (42), respectively, where satellite regions are plentiful. Correlations between the clustering based on Infinium assay and copy number alterations should be further examined.

Taken together, the data suggest that in CIMP-positive clear cell RCCs belonging to Cluster B, DNA hypermethylation of distinct CpG islands participates even in the very early and precancerous stages. Such DNA methylation alterations occurring in the precancerous stages may induce more aggressive tumor phenotypes and poorer patient outcome in Cluster B. On the other hand, in the other pathway of renal carcinogenesis leading to clear cell RCCs in Cluster A, DNA hypomethylation may be a later event (Table I) than DNA hypermethylation on CpG islands. We are now performing exome, transcriptome and proteome analyses of RCCs belonging to both clusters. Such multilayer omics analyses may identify the upstream genetic events inducing DNA methylation profiles and key signal pathways that characterize Clusters A and B.

Supplementary material

Supplementary Figures S1–S5 and Tables S1–S5 can be found at http://carcin.oxfordjournals.org/.

Funding

Program for Promotion of Fundamental Studies in Health Sciences of the National Institute of Biomedical Innovation (NiBio); Grant-in-Aid for the Third Term Comprehensive 10-Year Strategy for Cancer Control from the Ministry of Health, Labor and Welfare of Japan; National Cancer Center Research and Development Fund; Grants-in-Aid for Scientific Research (B) and for Young Scientists (B) from the Japan Society for the Promotion of Science (JSPS).

Acknowledgements

Conflict of Interest Statement: None declared.

References

1. Ljungberg,B. *et al.* (2011) The epidemiology of renal cell carcinoma. *Eur. Urol.*, **60**, 615–621.
2. Arai,E. *et al.* (2011) Genetic and epigenetic alterations during renal carcinogenesis. *Int. J. Clin. Exp. Pathol.*, **4**, 58–73.
3. Baldewijns,M.M. *et al.* (2010) VHL and HIF signalling in renal cell carcinogenesis. *J. Pathol.*, **221**, 125–138.
4. Barrett,I.P. (2010) Cancer genome analysis informatics. *Methods Mol. Biol.*, **628**, 75–102.
5. Zhang,J. *et al.* (2011) International Cancer Genome Consortium Data Portal--a one-stop shop for cancer genomics data. *Database (Oxford)*, **2011**, bar026.
6. Brannon,A.R. *et al.* (2010) Renal cell carcinoma: where will the state-of-the-art lead us? *Curr. Oncol. Rep.*, **12**, 193–201.
7. Dalgliesh,G.L. *et al.* (2010) Systematic sequencing of renal carcinoma reveals inactivation of histone modifying genes. *Nature*, **463**, 360–363.
8. van Haaften,G. *et al.* (2009) Somatic mutations of the histone H3K27 demethylase gene UTX in human cancer. *Nat. Genet.*, **41**, 521–523.
9. Varela,I. *et al.* (2011) Exome sequencing identifies frequent mutation of the SWI/SNF complex gene PBRM1 in renal carcinoma. *Nature*, **469**, 539–542.
10. Baylin,S.B. *et al.* (2011) A decade of exploring the cancer epigenome - biological and translational implications. *Nat. Rev. Cancer*, **11**, 726–734.
11. Boumber,Y. *et al.* (2011) Epigenetics in cancer: what's the future? *Oncology (Williston Park)*, **25**, 220–226, 228.
12. Jones,P.A. *et al.* (2007) The epigenomics of cancer. *Cell*, **128**, 683–692.
13. Kanai,Y. (2010) Genome-wide DNA methylation profiles in precancerous conditions and cancers. *Cancer Sci.*, **101**, 36–45.
14. Arai,E. *et al.* (2010) DNA methylation profiles in precancerous tissue and cancers: carcinogenetic risk estimation and prognostication based on DNA methylation status. *Epigenomics*, **2**, 467–481.
15. Kanai,Y. (2008) Alterations of DNA methylation and clinicopathological diversity of human cancers. *Pathol. Int.*, **58**, 544–558.
16. Kanai,Y. *et al.* (2007) Alterations of DNA methylation associated with abnormalities of DNA methyltransferases in human cancers during transition from a precancerous to a malignant state. *Carcinogenesis*, **28**, 2434–2442.
17. Arai,E. *et al.* (2008) Genetic clustering of clear cell renal cell carcinoma based on array-comparative genomic hybridization: its association with DNA methylation alteration and patient outcome. *Clin. Cancer Res.*, **14**, 5531–5539.
18. Arai,E. *et al.* (2006) Regional DNA hypermethylation and DNA methyltransferase (DNMT) 1 protein overexpression in both renal tumors and corresponding nontumorous renal tissues. *Int. J. Cancer*, **119**, 288–296.
19. Arai,E. *et al.* (2009) Genome-wide DNA methylation profiles in both precancerous conditions and clear cell renal cell carcinomas are correlated with malignant potential and patient outcome. *Carcinogenesis*, **30**, 214–221.
20. Arai,E. *et al.* (2011) Genome-wide DNA methylation profiles in renal tumors of various histological subtypes and non-tumorous renal tissues. *Pathobiology*, **78**, 1–9.
21. Bibikova,M. *et al.* (2009) Genome-wide DNA methylation profiling using Infinium® assay. *Epigenomics*, **1**, 177–200.
22. Eble,J.N. *et al.* (2004) Renal cell carcinoma. *World Health Organization Classification of Tumours. Pathology and Genetics. Tumours of the Urinary System and Male Genital Organs*. IARC Press, Lyon, pp. 10–43.
23. Fuhrman,S.A. *et al.* (1982) Prognostic significance of morphologic parameters in renal cell carcinoma. *Am. J. Surg. Pathol.*, **6**, 655–663.
24. Sobin,L.H. *et al.* (2002) International Union Against Cancer (UICC). *TNM Classification of Malignant Tumors*. 6th edn. Wiley-Liss, New York, pp. 193–195.
25. Kanai,T. *et al.* (1987) Pathology of small hepatocellular carcinoma. A proposal for a new gross classification. *Cancer*, **60**, 810–819.
26. Sambrook,J. *et al.* (2001) *Molecular Cloning: A Laboratory Manual*. 3rd edn. Cold Spring Harbor Laboratory Press, Cold Spring Harbor, NY, pp. 6.14–6.15.
27. Breiman,L. (2001) Random forests. *Mach. Learn.*, **45**, 5–32.
28. Morris,M.R. *et al.* (2010) Epigenetics of renal cell carcinoma: the path towards new diagnostics and therapeutics. *Genome Med.*, **2**, 59.
29. McRonald,F.E. *et al.* (2009) CpG methylation profiling in VHL related and VHL unrelated renal cell carcinoma. *Mol. Cancer*, **8**, 31.
30. Issa,J.P. (2004) CpG island methylator phenotype in cancer. *Nat. Rev. Cancer*, **4**, 988–993.
31. Toyota,M. *et al.* (1999) CpG island methylator phenotype in colorectal cancer. *Proc. Natl. Acad. Sci. U.S.A.*, **96**, 8681–8686.
32. Shen,L., *et al.* (2007) Integrated genetic and epigenetic analysis identifies three different subclasses of colon cancer. *Proc. Natl. Acad. Sci. U.S.A.*, **104**, 18654–18659.
33. Toyota,M. *et al.* (1999) Aberrant methylation in gastric cancer associated with the CpG island methylator phenotype. *Cancer Res.*, **59**, 5438–5442.
34. Nagashio,R. *et al.* (2011) Carcinogenetic risk estimation based on quantification of DNA methylation levels in liver tissue at the precancerous stage. *Int. J. Cancer*, **129**, 1170–1179.
35. Gotoh,M. *et al.* (2011) Diagnosis and prognostication of ductal adenocarcinomas of the pancreas based on genome-wide DNA methylation profiling by bacterial artificial chromosome array-based methylated CpG island amplification. *J. Biomed. Biotechnol.*, **2011**, 780–836.
36. Nishiyama,N. *et al.* (2010) Genome-wide DNA methylation profiles in urothelial carcinomas and urothelia at the precancerous stage. *Cancer Sci.*, **101**, 231–240.
37. Arai,E. *et al.* (2009) Genome-wide DNA methylation profiles in liver tissue at the precancerous stage and in hepatocellular carcinoma. *Int. J. Cancer*, **125**, 2854–2862.
38. Abe,M. *et al.* (2008) Identification of genes targeted by CpG island methylator phenotype in neuroblastomas, and their possible integrative involvement in poor prognosis. *Oncology*, **74**, 50–60.
39. Eden,A. *et al.* (2003) Chromosomal instability and tumors promoted by DNA hypomethylation. *Science*, **300**, 455.
40. Hansen,R.S. *et al.* (1999) The DNMT3B DNA methyltransferase gene is mutated in the ICF immunodeficiency syndrome. *Proc. Natl. Acad. Sci. U.S.A.*, **96**, 14412–14417.
41. Wong,N. *et al.* (2001) Hypomethylation of chromosome 1 heterochromatin DNA correlates with q-arm copy gain in human hepatocellular carcinoma. *Am. J. Pathol.* **59**, 465–471.
42. Nakagawa,T. *et al.* (2005) DNA hypomethylation on pericentromeric satellite regions significantly correlates with loss of heterozygosity on chromosome 9 in urothelial carcinomas. *J. Urol.*, **173**, 243–246.

Received December 11, 2012; revised April 17, 2012; accepted May 11, 2012

OPEN ACCESS Freely available online

PLOS | ONE

DNA Methylation Profiles at Precancerous Stages Associated with Recurrence of Lung Adenocarcinoma

Takashi Sato[1,2], Eri Arai[1]*, Takashi Kohno[3], Koji Tsuta[4], Shun-ichi Watanabe[5], Kenzo Soejima[2], Tomoko Betsuyaku[2], Yae Kanai[1]

1 Division of Molecular Pathology, National Cancer Center Research Institute, Tokyo, Japan, **2** Division of Pulmonary Medicine, Department of Medicine, Keio University School of Medicine, Tokyo, Japan, **3** Division of Genome Biology, National Cancer Center Research Institute, Tokyo, Japan, **4** Department of Pathology and Clinical Laboratories, Pathology Division, National Cancer Center Hospital, Tokyo, Japan, **5** Department of Thoracic Oncology, Thoracic Surgery Division, National Cancer Center Hospital, Tokyo, Japan

Abstract

The aim of this study was to clarify the significance of DNA methylation alterations at precancerous stages of lung adenocarcinoma. Using single-CpG resolution Infinium array, genome-wide DNA methylation analysis was performed in 36 samples of normal lung tissue obtained from patients without any primary lung tumor, 145 samples of non-cancerous lung tissue (N) obtained from patients with lung adenocarcinomas, and 145 samples of tumorous tissue (T). Stepwise progression of DNA methylation alterations from normal lung tissue to non-cancerous lung tissue obtained from patients with lung adenocarcinomas, and then tumorous tissue samples, was observed at 3,270 CpG sites, suggesting that non-cancerous lung tissue obtained from patients with lung adenocarcinomas was at precancerous stages with DNA methylation alterations. At CpG sites of 2,083 genes, DNA methylation status in samples of non-cancerous lung tissue obtained from patients with lung adenocarcinomas was significantly correlated with recurrence after establishment of lung adenocarcinomas. Among such recurrence-related genes, 28 genes are normally unmethylated (average β-values based on Infinium assay in normal lung tissue samples was less than 0.2) and their DNA hypermethylation at precancerous stages was strengthened during progression to lung adenocarcinomas ($\Delta\beta_{T-N}>0.1$). Among these 28 genes, we focused on 6 for which implications in transcription regulation, apoptosis or cell adhesion had been reported. DNA hypermethylation of the *ADCY5, EVX1, GFRA1, PDE9A,* and *TBX20* genes resulted in reduced mRNA expression in tumorous tissue samples. 5-Aza-2′-deoxycytidine treatment of lung cancer cell lines restored the mRNA expression levels of these 5 genes. Reduced mRNA expression in tumorous tissue samples was significantly correlated with tumor aggressiveness. These data suggest that DNA methylation alterations at precancerous stages determine tumor aggressiveness and outcome through silencing of specific genes.

Citation: Sato T, Arai E, Kohno T, Tsuta K, Watanabe S-i, et al. (2013) DNA Methylation Profiles at Precancerous Stages Associated with Recurrence of Lung Adenocarcinoma. PLoS ONE 8(3): e59444. doi:10.1371/journal.pone.0059444

Editor: Bernard W Futscher, The University of Arizona, United States of America

Received September 25, 2012; **Accepted** February 14, 2013; **Published** March 27, 2013

Funding: This study was supported by the Program for Promotion of Fundamental Studies in Health Sciences of the National Institute of Biomedical Innovation (NiBio, 10–42, http://www.nibio.go.jp/part/promote/fundamental/doc/index.html) and partially supported by a Grant-in-Aid for the Third Term Comprehensive 10-Year Strategy for Cancer Control from the Ministry of Health, Labor and Welfare of Japan (2, http://www.mhlw.go.jp/bunya/kenkyuujigyou/hojokin-koubo14/09.html), National Cancer Center Research and Development Fund (23-A-11, http://www.ncc.go.jp/jp/about/rinri/kaihatsu/files/h24_ncc_research_list.pdf), and Grants-in-Aid for Scientific Research (B, 233900 90, http://www.jsps.go.jp/j-grantsinaid/) and for Young Scientists (B, 23790456, http://www.jsps.go.jp/j-grantsinaid/) from the Japan Society for the Promotion of Science (JSPS). National Cancer Center Biobank is supported by the National Cancer Center Research and Development Fund (23-A-1, http://www.ncc.go.jp/jp/about/rinri/kaihatsu/files/h24_ncc_research_list.pdf), Japan. T. Sato is an awardee of a research resident fellowship from the Foundation for Promotion of Cancer Research in Japan (http://www.fpcr.or.jp/index.html). The funders had no role in study design, data collection and analysis, decision to publish, or preparation of the manuscript.

Competing Interests: The authors have declared that no competing interests exist.

* E-mail: earai@ncc.go.jp

Introduction

Lung adenocarcinoma (LADC) is increasingly recognized as a clinicopathologically and molecularly heterogeneous disease: frequent mutations of the *EGFR, KRAS, BRAF, TP53, ERBB2, PIK3CA* and *MET* genes and *EML4-ALK* fusions have been reported in LADCs [1,2]. In addition, recent whole-exome sequencing has revealed frequent mutation of the *CSMD3* gene [3]. However, the molecular background responsible for the clinicopathological diversity of LADCs is not yet fully understood.

As well as genetic abnormalities, epigenetic changes in human cancers have also been described [4–7]. In LADCs, silencing of the *RASSF1A, CDKN2A, RARβ, MGMT, APC, DAPK, FHIT* and *CDH13* genes due to DNA hypermethylation around their promoter regions has been frequently observed [8]. In addition, DNA methylation alterations are known to occur even at the early and precancerous stages of carcinogenesis in various organs [5–7,9]. For example, we have reported that DNA hypermethylation at the D17S5 locus, where the *HIC-1* tumor suppressor gene has been identified, is evident even in non-cancerous lung tissue obtained from patients with non-small cell lung cancers, and is correlated with smoking history [10]. Other researchers have also reported DNA hypermethylation of specific tumor-related genes at precancerous stages associated with cigarette smoking [8,11]. However, it has been unclear whether DNA methylation status is simply altered at precancerous stages or whether DNA methylation alterations at these stages actually result in gene expression alterations in established LADCs. Moreover, in organs other than

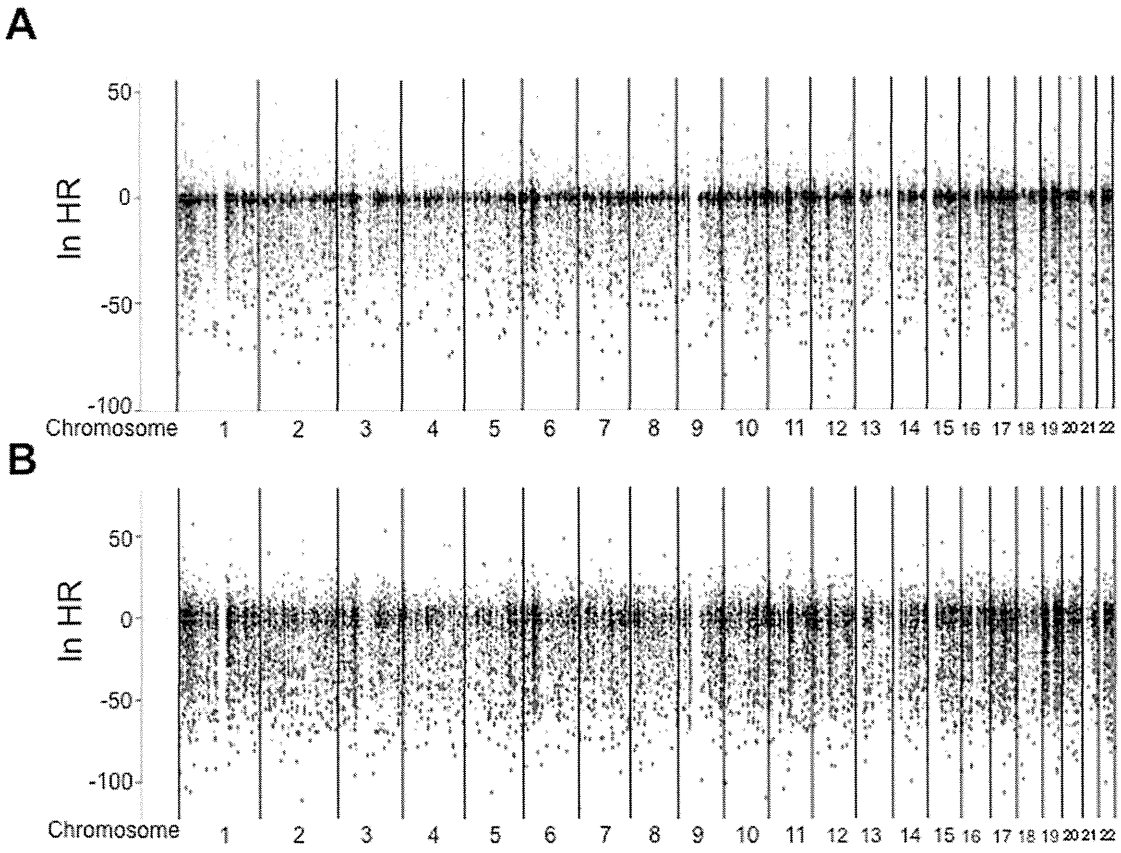

Figure 1. Hazard ratio (HR) obtained from the Cox regression model. Correlation between DNA methylation status (average β-values) and recurrence was examined in 145 samples of tumorous tissue (**A**) and 145 samples of the corresponding non-cancerous lung tissue (**B**) obtained from patients with lung adenocarcinomas who had undergone complete resection and had not received any adjuvant therapy after surgery. All of the examined 26,455 probes of the Infinium array are shown along the chromosomes. Red color means that higher β-values of the probes were observed in recurrence-positive patients than in recurrence-negative patients ($P<0.001$). Blue color means that lower β-values of the probes were observed in recurrence-positive patients than in recurrence-negative patients ($P<0.001$).
doi:10.1371/journal.pone.0059444.g001

the lung, it has been suggested that DNA methylation profiles at precancerous stages may determine tumor aggressiveness and outcome [12–14]. However, the clinicopathological impact of DNA methylation alterations at precancerous stages during lung carcinogenesis has not been clarified.

Recently, genome-wide DNA methylation analysis using the single-CpG resolution Infinium array has made it possible to interrogate 27,000 highly informative CpG sites, i.e. an average of two CpG sites within the proximal promoter regions of the transcription start sites of each of 14,475 consensus coding sequences in the National Center for Biotechnology Information Database, especially 3 to 20 CpG sites for more than 200 cancer-related and imprinted genes [15]. Although a few studies of lung cancers employing the Infinium assay have been reported [16,17], they did not focus on precancerous stages. In order to clarify the significance of DNA methylation alterations at precancerous stages of lung carcinogenesis, we performed the Infinium assay in association with mRNA expression and clinicopathological analyses of 36 samples of normal lung tissue (C) obtained from patients without any primary lung tumors, 145 samples of non-cancerous lung tissue (N) from patients with LADCs, and 145 corresponding samples of tissue from the tumors (T) themselves. Although the molecular classification of LADCs based on the results of the Infinium assay will be published elsewhere, we focused on specific genes methylated at precancerous stages in the present study.

Materials and Methods

Patients and Tissue Samples

The 145 paired samples of N and the corresponding T were obtained from patients with primary LADCs who underwent lung resection at the National Cancer Center Hospital, Japan, between December 1997 and March 2008. These patients had undergone complete resection and had not received any preoperative treatment or adjuvant therapy after surgery. Eighty-one patients were males and 64 were females with a median age of 61 years (range, 30–81 yr). Histological diagnosis and grading were based on the 2004 World Health Organization classification [18]. Recurrence was diagnosed by clinicians on the basis of physical examination and imaging modalities such as computed tomography, magnetic resonance imaging, scintigraphy or positron-emission tomography, and sometimes confirmed histopathologically by biopsy.

For comparison, 36 C samples were obtained from materials that had been surgically resected from patients without any primary lung tumor. Twenty-two of these patients were males and 14 were females, with a median age of 63 years (range, 27–83 yr).

Table 1. The 28 probes for which the average β-value in N samples (β_N) was higher in recurrence-positive patients than in recurrence-negative patients, for which the average β-value in C samples (β_C) was less than 0.2, and for which the average β-value in T samples minus that in corresponding N samples ($\Delta\beta_{T-N}$) was more than 0.1.

Target ID[a]	Chromosome	Position[b]	Gene symbol	P[c]	Adjusted P[d]
cg00516481	21	44,073,202	*PDE9A*	9.996×10^{-4}	1.193×10^{-2}
cg01295203	8	70,984,199	*PRDM14*	8.156×10^{-5}	3.236×10^{-3}
cg02008154	7	35,293,537	*TBX20*	7.188×10^{-4}	9.917×10^{-3}
cg02909790	6	26,271,587	*HIST1H3G*	2.896×10^{-6}	5.787×10^{-4}
cg03538436	12	117,799,370	*NOS1*	7.227×10^{-4}	9.944×10^{-3}
cg03963198	5	1,882,871	*IRX4*	5.133×10^{-4}	8.186×10^{-3}
cg06005396	19	590,541	*HCN2*	9.485×10^{-4}	1.158×10^{-2}
cg06269753	8	72,755,871	*MSC*	8.627×10^{-7}	3.426×10^{-4}
cg07651242	7	45,614,720	*ADCY1*	7.403×10^{-4}	1.010×10^{-2}
cg11612345	6	168,842,491	*SMOC2*	4.264×10^{-6}	6.753×10^{-4}
cg12087643	10	118,033,370	*GFRA1*	3.144×10^{-9}	2.489×10^{-5}
cg12265829	14	24,804,022	*ADCY4*	7.265×10^{-4}	9.984×10^{-3}
cg13262687	4	147,559,579	*POU4F2*	6.246×10^{-5}	2.795×10^{-3}
cg13449778	1	179,712,298	*FAM163A*	8.195×10^{-7}	3.426×10^{-4}
cg13878010	3	123,167,276	*ADCY5*	2.339×10^{-6}	5.220×10^{-4}
cg16254309	7	145,814,152	*CNTNAP2*	2.917×10^{-4}	6.240×10^{-3}
cg16387606	1	149,804,293	*HIST2H4A*	7.441×10^{-4}	1.011×10^{-2}
cg16604516	3	13,590,419	*FBLN2*	7.181×10^{-4}	9.916×10^{-3}
cg16652259	2	172,949,501	*DLX1*	4.175×10^{-4}	7.386×10^{-3}
cg17191178	3	157,824,217	*SHOX2*	8.872×10^{-5}	3.353×10^{-3}
cg18454685	17	48,639,239	*CACNA1G*	4.326×10^{-4}	7.487×10^{-3}
cg20286200	6	133,562,267	*EYA4*	1.541×10^{-9}	2.038×10^{-5}
cg21087137	12	75,728,469	*GLIPR1L1*	1.965×10^{-6}	4.821×10^{-4}
cg22461835	8	26,723,365	*ADRA1A*	7.297×10^{-4}	9.998×10^{-3}
cg23418591	20	57,090,317	*LOC149773*	4.075×10^{-4}	7.287×10^{-3}
cg25302419	5	11,904,015	*CTNND2*	5.149×10^{-4}	8.194×10^{-3}
cg25764191	10	105,037,215	*INA*	3.834×10^{-4}	7.026×10^{-3}
cg27626299	7	27,282,431	*EVX1*	2.164×10^{-4}	5.423×10^{-3}

[a]Probe ID for the Infinium HumanMethylation27 Bead Array (Illumina).
[b]National Center for Biotechnology Information database (Genome Build 37).
[c]Non-adjusted *P*-values and.
[d]Benjamini-Hochberg-adjusted *P*-values for the Cox regression model used for evaluation of correlation with recurrence.
doi:10.1371/journal.pone.0059444.t001

Thirty-five had undergone lung resection for metastatic lesions of primary cancers of the colon, rectum, kidney, urinary bladder, thyroid, breast, pancreas, ampulla of Vater and salivary gland, osteosarcoma, synovial sarcoma, leiomyosarcoma, rhabdmyosarcoma, liposarcoma, dermatofibrosarcoma, and myxofibrosarcoma. The remaining one patient had undergone chest wall resection for lipoma with removal of adjacent lung tissue. Histological observation confirmed that all of the C samples showed no remarkable histological abnormality and did not contain any contaminating tumor cells that had metastasized from organs other than the lung.

Tissue specimens were provided by the National Cancer Center Biobank, Japan. This study was approved by the Ethics Committee of the National Cancer Center, Tokyo, Japan, and was performed in accordance with the Declaration of Helsinki 1975. All patients included in this study provided written informed consent.

Cell Lines

The characteristics of the four lung cancer cell lines used in this study are summarized in Table S1.

Infinium Assay

Genomic DNA was extracted using a QIAamp DNA Mini kit (Qiagen, Valencia, CA, USA) and phenol-chloroform extraction followed by dialysis [19] from all tissue samples and cell lines, respectively. Five-hundred-nanogram aliquots of DNA were subjected to bisulfite conversion using an EZ DNA Methylation-Gold Kit (Zymo Research, Irvine, CA, USA). DNA methylation status at 27,578 CpG loci was examined at single-CpG resolution using the Infinium HumanMethylation27 Bead Array (Illumina, San Diego, CA, USA). After hybridization, the specifically hybridized DNA was fluorescence-labeled by a single-base extension reaction and detected using a BeadScan reader (Illumina) in accordance with the manufacturer's protocols. The data were then assembled using GenomeStudio methylation

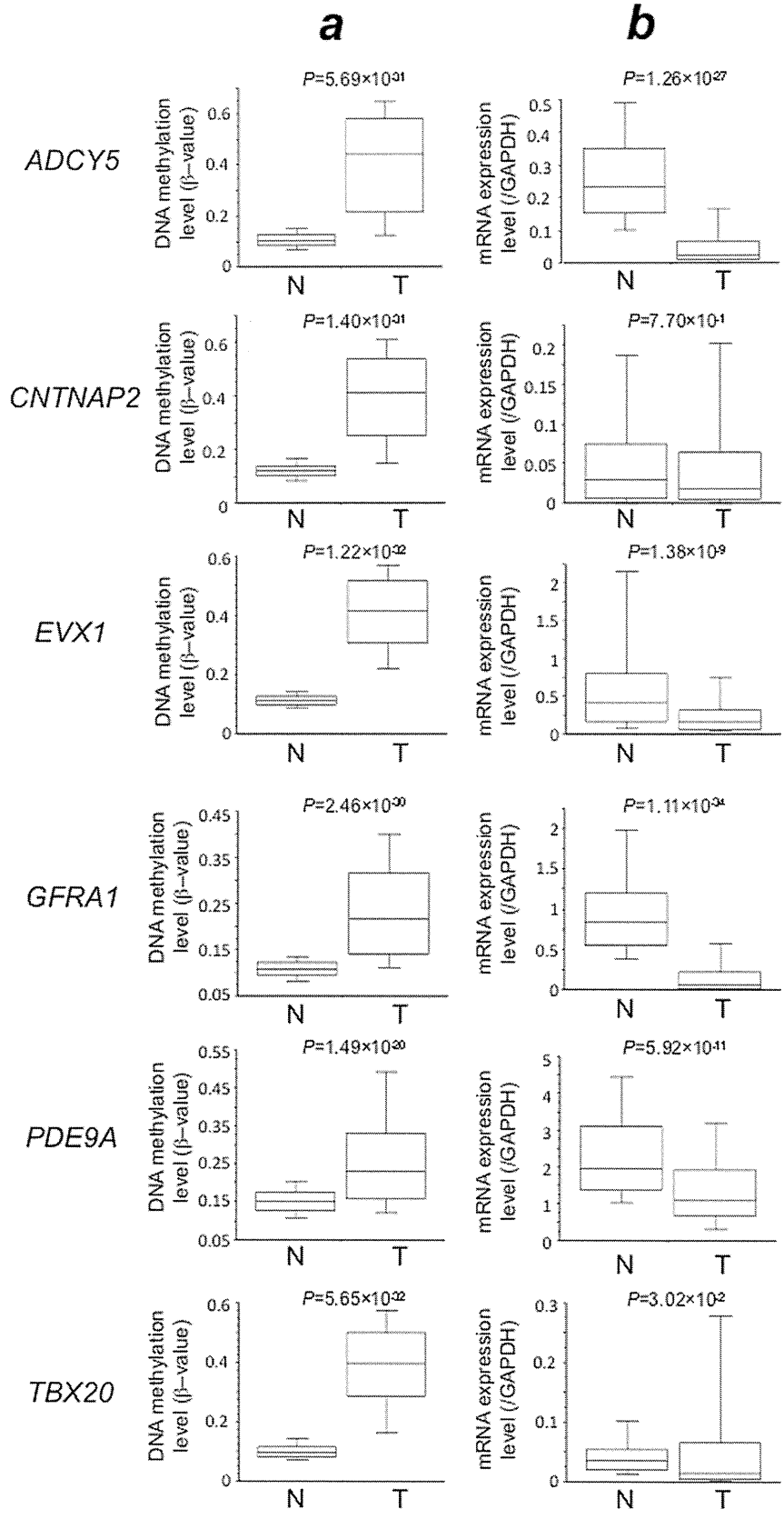
a
b
ADCY5
CNTNAP2
EVX1
GFRA1
PDE9A
TBX20
P=5.69×10-31
P=1.26×10-27
P=1.40×10-31
P=7.70×10-1
P=1.22×10-32
P=1.38×10-9
P=2.46×10-30
P=1.11×10-34
P=1.49×10-30
P=5.92×10-11
P=5.65×10-32
P=3.02×10-2
DNA methylation level (β-value)
mRNA expression level (/GAPDH)
N
T

Figure 2. Correlation between DNA methylation levels and mRNA expression levels. DNA methylation levels (average β-values) (**A**) and mRNA expression levels (**B**) for the *ADCY5, CNTNAP, EVX1, GFRA1, PDE9A* and *TBX20* genes in samples of non-cancerous lung tissue (N) from patients with lung adenocarcinomas and samples of the corresponding tumorous tissue (T) were determined by Infinium assay and quantitative real-time reverse transcription-PCR analysis, respectively. DNA methylation levels for all six genes were significantly higher in T samples than in N samples, and levels of expression of mRNAs for the *ADCY5, EVX1, GFRA1, PDE9A* and *TBX20* genes were significantly lower in T samples than in N samples, although the reduction in the expression of the *CNTNAP2* gene did not reach statistical significance. These results suggested that DNA hypermethylation of the *ADCY5, EVX1, GFRA1, PDE9A* and *TBX20* genes may result in reduced mRNA expression in tissue samples from the same cohort.
doi:10.1371/journal.pone.0059444.g002

software (Illumina). At each CpG site, the ratio of the fluorescence signal was measured using a methylated probe relative to the sum of the methylated and unmethylated probes, i.e. the so-called β-value, which ranges from 0.00 to 1.00, reflecting the methylation level of an individual CpG site.

Quantitative Real-time Reverse Transcription (RT)-PCR Analysis

Total RNA was extracted from 132 N and 151 T samples for which additional tissue specimens were available and cell lines using TRIzol reagent (Life Technologies, Carlsbad, CA, USA) in accordance with the manufacturer's instructions. cDNA was synthesized from total RNA with random primers using SuperScript III Reverse Transcriptase (Life Technologies) and pre-amplified using TaqMan PreAmp Master Mix (Life Technologies).

To evaluate mRNA expression levels, fluorescence-labeled locked nucleic acid hydrolysis probes were selected from the Universal Probe Library collection (Roche Applied Science, Mannheim, Germany) and specific PCR primers yielding intron-spanning amplicons were designed using ProbeFinder assay design software (https://www.roche-applied-science.com/sis/rtpcr/upl/index.jsp?id = UP030000). The probe ID and primer sequences are summarized in Table S2. Quantitative real-time PCR was performed using TaqMan Universal Master Mix II (Life Technologies) and the relative standard curve method in the BioMark HD System (Fluidigm, South San Francisco, CA, USA). Ct values were normalized to that of *GAPDH* in the same sample. All assays were performed in triplicate.

5-aza-2′-deoxycytidine (5-aza-dC) Treatment

A549, PC9, VMRC-LCD and EBC-1 cells were seeded at a density of 9×10^5 cells per 15-cm dish on day 0 and then allowed to attach for a 24-h period. Then, 5-aza-dC (Sigma-Aldrich, St. Louis, MO, USA) was added to a final concentration of 1 μM. Cells were passaged at a subculture ratio of 1:2 on day 3. At 24 h after replating, 5-aza-dC was added again to the same final concentration. Since toxicity had been obvious during preliminary experiments, the final concentration of 5-aza-dC was reduced to 0.1 μM for EBC-1 cells. Genomic DNA and total RNA were extracted from all cells on days 3 and 6.

Statistics

In the Infinium assay, all CpG sites on chromosomes X and Y were excluded, to avoid any gender-specific methylation bias. The call proportions (*P*-values for detection of signals above the background <0.01) for 31 probes (shown in Table S3) in all of the tissue samples examined were less than 90%. Since such a low proportion may be attributable to polymorphism at the probe CpG sites, these 31 probes were excluded from the present assay, leaving a final total of 26,455 autosomal CpG sites.

Infinium probes showing ordered differences from 36 C to 145 N, and then to the 145 T samples themselves, were examined by the cumulative logit model adjusted by sex, age and experimental batch ($P<1\times10^{-14}$). Correlations between β-values in N and T samples and recurrence were assessed by the Cox regression model adjusted by sex, age and experimental batch ($P<0.001$). Benjamini-Hochberg correction was performed to adjust for multiple testing. Differences of β-values and mRNA expression levels between N and T samples were examined by Mann-Whitney U test. Correlations between mRNA expression levels and clinicopathological parameters were assayed by analysis of variance between groups (ANOVA) and Welch's T-test: after adjusted Bonferroni correction to adjust for multiple testing, corrected *P* values of <0.05 were considered to be significant. All statistical analyses were performed using programming language R.

Results

DNA Methylation Profiles Associated with Recurrence are Established at Precancerous Stages

DNA methylation levels of CpG sites of the *CNTNAP2*, *EVX1*, *GFRA1*, *PDE9A* and *TBX20* genes based on the Infinium assay were clearly verified using the quantitative pyrosequencing method (Figure S1), indicating the reliability of the Infinium assay. The cumulative logit model ($P<1\times10^{-14}$) revealed ordered progression of DNA methylation alterations from C to N, and then to T samples, on 3,270 probes; DNA methylation alterations occurred even in N samples compared to C samples, and such DNA methylation alterations were inherited by, or strengthened in, T samples, indicating that Ns were at precancerous stages with DNA methylation alterations. Among the 3,270 probes, the number showing average β-values in T samples minus average β-values in C samples ($\Delta\beta_{T\text{-}C}$) of >0.1 and <−0.1 were 1,209 and 1,056, respectively. Thus, when we defined differentially methylated probes as probes showing a $\Delta\beta_{T\text{-}C}$ value of >0.1 or <−0.1, the false positivity rate by the cumulative logit model was 4.3%.

Correlations between DNA methylation status and recurrence were examined using the Cox regression model ($P<0.001$) for 145 patients. In T samples, DNA methylation status on 944 probes for the 916 genes was significantly correlated with recurrence: on 87 probes (red dots in Figure 1A), higher β-values were observed in recurrence-positive patients than in recurrence-negative patients, whereas lower β-values on 857 probes (blue dots in Figure 1A) were observed in recurrence-positive patients. Surprisingly, even in N samples, the DNA methylation status on 2,215 probes for the 2,083 genes was significantly correlated with recurrence: on 425 probes (red dots in Figure 1B), higher β-values were observed in recurrence-positive patients than in recurrence-negative patients, whereas lower β-values on 1,790 probes (blue dots in Figure 1B) were observed in recurrence-positive patients.

In order to identify recurrence-related genes that are normally unmethylated and for which DNA hypermethylation at precancerous stages is strengthened in the established LADCs, among the 425 probes (red dots in Figure 1B), we initially focused on 28 probes for which the average β-values in C samples (β_C) were less than 0.2 and the average β-values in T samples minus that in the corresponding N samples ($\Delta\beta_{T\text{-}N}$) were more than 0.1 (Table 1).

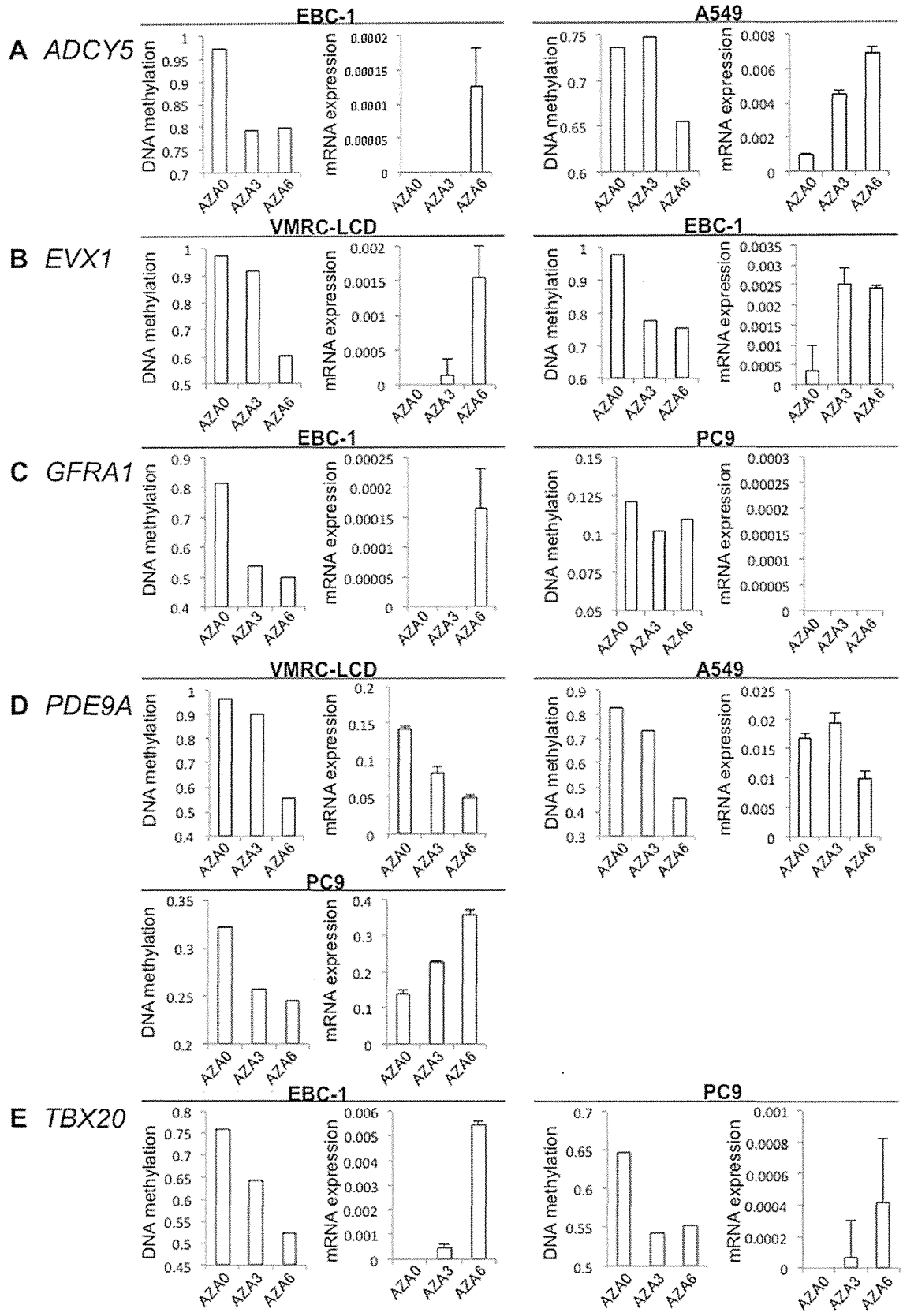
A ADCY5
EBC-1
A549
B EVX1
VMRC-LCD
EBC-1
C GFRA1
EBC-1
PC9
D PDE9A
VMRC-LCD
A549
PC9
E TBX20
EBC-1
PC9
DNA methylation
mRNA expression
AZA0
AZA3
AZA6

Figure 3. DNA methylation levels and mRNA expression levels after 5-aza-2′-deoxycytidine (5-aza-dC) treatment. DNA methylation levels (β-values) and mRNA expression levels for the *ADCY5* (**A**), *EVX1* (**B**), *GFRA1* (**C**), *PDE9A* (**D**) and *TBX20* (**E**) genes were determined by Infinium assay and quantitative real-time reverse transcription-PCR analysis, respectively. The error bars represent the standard deviation for triplicate quantitative real-time RT-PCR analyses. DNA methylation levels and mRNA expression levels on days 3 (AZA3) and 6 (AZA6) were compared with those of untreated cells (AZA0). After 5-aza-dC treatment, reduction of DNA methylation levels and restoration of the mRNA expression levels of *ADCY5* (**A**), *EVX1* (**B**) and *TBX20* (**E**) were observed in both of the cell lines used. In panel **C**, since reduction of the DNA methylation level was not induced by 5-aza-dC in PC9 cells, restoration of mRNA expression did not occur in these cells. Panel **D** shows reduction of the DNA methylation level and restoration of the mRNA expression level in PC9 cells.
doi:10.1371/journal.pone.0059444.g003

Silencing of Recurrence-related Genes due to DNA Hypermethylation

Among the 28 genes listed in Table 1, we further focused on 6 genes (*ADCY5* [20,21], *CNTNAP2* [22,23], *EVX1* [24], *GFRA1* [25], *PDE9A* [26,27] and *TBX20* [28]) for which implications in transcription regulation, apoptosis or cell adhesion had been reported. Quantitative real-time RT-PCR analysis of these 6 genes was performed in 132 N and 151 T samples for which total RNA was available. mRNA expression levels for the *ADCY5, EVX1, GFRA1, PDE9A* and *TBX20* genes in T samples were significantly lower than those in N samples, although the reduced expression of the *CNTNAP2* gene did not reach statistical significance (Figure 2B). The DNA methylation statuses (β-values in N and T samples) of the 6 genes are also shown in Figure 2A; the data suggested that DNA hypermethylation of these genes might result in reduction of mRNA expression in tissue samples from the same cohort.

DNA methylation levels of the *ADCY5, EVX1, GFRA1, PDE9A* and *TBX20* genes in lung cancer cell lines A549, PC9, VMRC-LCD and EBC-1 are shown in Figure S2. To examine the effects of the DNA methylation inhibitor, the top two cell lines showing the highest DNA methylation levels (β-values) were selected for each gene. In fact, mRNA expression levels determined by quantitative real-time RT-PCR analysis of the genes (with the exception of PDE9A) were extremely low in the cell lines selected. 5-aza-dC treatment induced marked reduction of DNA methylation levels and restored the mRNA expression levels of *ADCY5, EVX1, GFRA1* and *TBX20* (Figure 3). With regard to *GFRA1*, since reduction of the DNA methylation level was not induced by 5-aza-dC, restoration of mRNA expression did not occur in PC9 cells. Taken together with Figures 2 and 3, the data suggested that the examined genes were silenced due to DNA hypermethylation in the lung cancers. With regard to *PDE9A*, for which the mRNA expression levels were high even in the top two cell lines showing the highest levels of DNA methylation, 5-aza-dC treatment did not further increase the mRNA expression level in the two cell lines. The PC9 cells were then additionally treated with 5-aza-dC, and restoration of *PDE9A* mRNA expression due to DNA demethylation was confirmed in the cells (Figure 3).

Clinicopathological Impact of Reduced Expression of mRNA for Recurrence-related Genes

Reduced expression of mRNA for *ADCY5, EVX1, GFRA1* and *PDE9A* in T samples was correlated with clinicopathological parameters reflecting tumor aggressiveness, such as a larger tumor diameter, higher histological grade, blood vessel invasion, pleural invasion and tumor anthracosis (Table 2), although their mRNA expression levels were not predictors of recurrence that were independent of known parameters such as pathological-TNM stage and lymph node metastasis (Table S4). With regard to the correlation with histological subtype, levels of mRNA expression for *GFRA1* and *PDE9A* were significantly higher in lepidic-type LADCs showing a less invasive growth pattern than in other histological subtypes.

Discussion

The 'field cancerization' phenomenon in the lung has become evident, being especially associated with cigarette smoking [31]. We and other groups have reported DNA methylation of specific genes or chromosomal loci in non-cancerous lung tissue obtained from lung cancer patients, or in lung tissue from cancer-free smokers [8–10]. These previous data drew our attention to DNA methylation alterations at precancerous stages of LADC. However, the impact of DNA methylation alterations at precancerous stages on the expression of specific gene and clinicopathological parameters of established cancers has remained unclear. Moreover, previous examinations focusing on precancerous stages in the lung have not involved a genome-wide approach. Although Selamat et al. and Lockwood et al. have reported Infinium assay results for 59 and 43 lung cancer samples, respectively [16,17], they did not focus on precancerous stages.

Here we have reported the results of the Infinium assay for 326 lung tissue samples including 145 N samples. Our cumulative logit model analysis revealed stepwise progression of DNA methylation alterations from C to N, and then T samples on 3,270 probes. Genome-wide analysis at single-CpG resolution confirmed that DNA methylation alterations actually occurred even at precancerous stages, although the possibility that such alterations observed in N samples had been influenced by differences in tissue composition between C and N samples cannot be completely excluded. Moreover, it was clearly shown that such DNA methylation alterations had clinicopathological impact, since many probes in N samples were significantly correlated with recurrence after establishment of LADCs (Figure 1B). DNA methylation profiles determining outcome are already established at precancerous stages. The finding that the number of probes showing DNA methylation alterations significantly associated with recurrence in N samples was larger than that in T samples may have been due to the fact that passenger DNA methylation alterations occurring during progression from the precancerous stages to established cancers may have masked any clinicopathologically significant DNA methylation profiles in T samples.

Next, we focused on 28 recurrence-related genes that are normally unmethylated and for which DNA hypermethylation in N samples was strengthened in T samples (Table 1). Among these 28 genes, we further focused on *ADCY5, CNTNAP2, EVX1, GFRA1, PDE9A* and *TBX20*, based on their previously reported implications in transcription regulation, apoptosis or cell adhesion. (a) The data in *adcy5*-knockout mice indicated that ADCY5 promotes apoptosis in cardiomyocytes [20,21]. Although large-scale screening studies of leukemias have identified *ADCY5* as one of the genes that are methylated in leukemic cells [32,33], the clinicopathological impact of DNA methylation of the *ADCY5* gene has not yet been clarified in human malignancies. (b) CNTNAP2, a glial adhesion molecule, binds extracellularly to contactin 2, an immunoglobulin superfamily neural recognition protein [22]. *CNTNAP2* is known to be a tumor-suppressor gene for gliomas, and is disrupted by chromosomal translocations and gene mutations [23]. Although a large-scale screening study of

Table 2. Correlation between mRNA expression levels of recurrence-related genes and clinicopathological factors.

Clinicopathological parameters	Number of tumors	*ADCY5*		*EVX1*		*GFRA1*		*PDE9A*		*TBX20*	
		Expression[a]	P^b	Expression[a]	P^b	Expression[a]	P^b	Expression[a]	P^b	Expression[a]	P^b
Tumor diameter											
<2.5 cm	43	−4.95±2.10	1.63×10^{-1c}	−2.80±1.82	4.24×10^{-1c}	−3.27±2.67	1.60×10^{-3c}	0.50±1.39	3.40×10^{-2c}	−5.73±2.68	7.65×10^{-1c}
≥2.5 cm, <4 cm	61	−5.25±2.39		−2.36±2.16		−4.02±2.86		0.28±1.76		−5.76±2.78	
≥4 cm	47	−6.14±2.76		−3.04±2.02		−5.74±3.28		−0.50±1.59		−6.10±2.84	
Histological subtype[d]											
Lepidic	12	−4.19±1.61	2.10×10^{-1c}	−2.73±2.14	1.79×10^{-1c}	−1.64±2.35	1.71×10^{-4c}	0.93±1.07	1.73×10^{-3c}	−6.24±1.79	1.28×10^{-1c}
Acinar	24	−6.03±2.01		−2.91±2.09		−5.41±2.72		−0.20±1.36		−5.77±2.57	
Papillary	69	−5.30±2.35		−2.29±1.99		−3.90±2.65		0.23±1.63		−5.28±2.80	
Micropapillary	15	−4.69±2.19		−2.35±2.10		−3.47±2.87		1.20±1.27		−6.89±1.79	
Solid	28	−6.34±3.24		−3.62±1.88		−6.27±3.62		−0.91±1.81		−6.37±3.11	
Invasive mucinous	3	−4.64±1.46		−3.19±1.24		−2.95±1.43		0.16±1.68		−8.21±0.14	
Histological grades											
G1	56	−4.60±1.80	1.28×10^{-3c}	−2.68±1.90	4.57×10^{-2c}	−2.62±1.93	4.80×10^{-10}	0.55±1.41	1.32×10^{-4}	−5.48±2.69	9.50×10^{-2}
G2	65	−5.58±2.33		−2.32±2.10		−4.59±2.71		0.25±1.57		−5.74±2.67	
G3	30	−6.73±3.20		−3.54±1.92		−7.01±3.60		−1.06±1.77		−6.81±2.94	
Lymphatic invasion											
Negative	52	−5.31±2.43	1.00[e]	−2.76±1.71	1.00[e]	−3.95±3.38	1.00[e]	0.06±1.64	1.00[e]	−5.86±2.42	9.82×10^{-1e}
Positive	99	−5.52±2.50		−2.66±2.19		−4.55±2.92		0.12±1.67		−5.85±2.93	
Blood vessel invasion											
Negative	43	−4.89±2.40	2.38×10^{-1e}	−2.77±1.84	7.68×10^{-1e}	−3.13±3.45	2.81×10^{-2e}	0.63±1.68	6.39×10^{-2e}	−5.71±2.60	1.00[e]
Positive	108	−5.66±2.47		−2.67±2.11		−4.82±2.81		−0.11±1.60		−5.92±2.83	
Pleural invasion											
Negative	78	−5.16±2.42	4.45×10^{-1c}	−2.77±2.15	4.60×10^{-1c}	−3.65±2.83	7.28×10^{-3c}	0.28±1.61	5.82×10^{-1c}	−5.95±2.51	5.38×10^{-1c}
Invasion to the visceral pleura beyond the elastic fiber	33	−5.88±2.68		−2.62±2.07		−4.99±3.54		0.03±1.93		−6.41±2.96	
Invasion to the surface of the visceral pleura	22	−4.96±2.07		−2.16±1.62		−4.01±2.66		0.18±1.29		−4.98±2.82	
Invasion to the parietal pleura	18	−6.47±2.49		−3.15±1.90		−6.56±2.71		−0.65±1.58		−5.52±3.22	
Tumor anthracosis [f]											
Negative	68	−4.97±2.57	8.27×10^{-2e}	−2.37±2.22	2.04×10^{-1e}	−3.32±2.80	1.08×10^{-3e}	0.70±1.46	1.66×10^{-4e}	−5.51±2.78	1.99×10^{-1e}
Positive	82	−5.87±2.30		−2.91±1.79		−5.10±3.02		−0.39±1.66		−6.09±2.69	

[a]Average of log2-transformed mRNA expression levels/GAPDH ± standard deviation. [b]Adjusted *P*-values using adjusted Bonferroni correction. [c]Analysis of variance between groups. [d]Predominant histological subtypes of LADCs were diagnosed according to the classification devised by the International Association for the Study of Lung Cancer, the American Thoracic Society and the European Respiratory Society [29]. [e]Welch's T-test. [f]Coal dust is accumulated in active fibroblast proliferation foci, which is associated with poorer prognosis of lung adenocarcinoma patients and reflects an active cancer-stromal interaction [30]. *P* values of <0.05 are underlined.

doi:10.1371/journal.pone.0059444.t002

pancreatic cancers has identified *CNTNAP2* as one of the genes that are methylated in cancer cells [34], the clinicopathological impact of DNA methylation of the *CNTNAP2* gene has not yet been elucidated in human malignancies. (c) *EVX1*, encoding a homeobox protein, functions as a potent repressor of gene transcription and plays an important role during mouse embryogenesis [24]. Although Truong et al. have recently suggested that DNA hypermethylation of the *EVX1* gene may be a predictor of recurrence of prostatic cancers [35], the implications of *EVX1* in human cancers other than prostatic cancer have been unclear. (d) GFRA1 is a receptor for glial cell-derived neurotrophic factor (GDNF) and enriched in the pre- and post-synaptic compartments. GDNF triggers trans-homophilic binding between GFRA1 molecules, resulting in adhesion between *GFRA1*-expressing cells [25]. Overexpression of *GFRA1* has been reported in chemotherapy-sensitive oligodendrogliomas [36]. Although Salamat et al. described *GFRA1* as one of the genes differentially methylated between cancerous and non-cancerous tissue obtained from lung cancer patients subclustered on the basis of DNA methylation profiles [16], the clinicopathological impact of DNA methylation of the *GFRA1* gene was not examined in LADCs. (e) *PDE9A* encodes cGMP-specific phosphodiesterase [26]. PDE9A inhibitor has been reported to induce apoptosis of breast cancer cell lines through caspase 3 activation [27]. On the other hand, breakpoints within the *PDE9A* gene have been frequently observed in B-cell precursor acute lymphoblastic leukemia [36]. However, the implications of DNA methylation in the regulation of *PDE9A* have never been reported in human malignancies or other diseases. (f) TBX20, a member of the T-box transcription factors, is a critical regulator of heart development, and mutations of the human *TBX20* gene result in cardiac malformations [28]. However, the implications of DNA methylation in *TBX20* regulation and of *TBX20* dysfunction in human malignancies have never been reported.

Among these 6 genes, DNA hypermethylation of the *ADCY5, EVX1, GFRA1, PDE9A* and *TBX20* genes was associated with reduced mRNA expression in tissue samples of the same cohort. 5-aza-dC treatment of human lung cancer cell lines restored the expression of the 5 genes, indicating that genes showing DNA hypermethylation at precancerous stages are actually silenced due to DNA hypermethylation during lung carcinogenesis. With regard to *PDE9A*, the level of mRNA expression was not necessarily low and was not always restored by 5-aza-dC treatment in any of the cell lines examined, indicating that DNA methylation is not the only mechanism responsible for *PDE9A* regulation in lung cancers. In addition, there are gaps between the timing of the reduction of DNA methylation and recovery of mRNA expression in *ADCY5* in EBC-1 cells and A549 cells and *GFRA1* in EBC-1 cells, again indicating the possibility that there are alternative mechanisms regulating the mRNA expression levels of these genes other than DNA methylation. Reduced expression of the mRNAs for the *ADCY5, EVX1, GFRA1* and *PDE9A* genes was significantly correlated with clinicopathological parameters (Table 2), indicating that DNA methylation alterations, even from the precancerous stage, ultimately determine the tumor phenotype through gene silencing.

Unlike the present study, which was conducted to clarify the significance of DNA methylation alterations at precancerous stages, many previous studies attempted to establish prognostic factors based on DNA methylation status using candidate gene approaches [37–41]. Microarray studies are generally considered to be useful for establishing prognostic biomarkers. In lung cancers, array-based DNA methylation screening [42] has been performed for prognostication. Next-generation sequencing associated with bioinformatics analysis [43] has also been reported for lung cancers. Such previous studies identified the *RASSF1A* [37], *PITX2* [38], *SHOX2* [38], *TFPI-2* [39], *FHIT* [40], *p16* [41], *CDH13* [41], and *APC* [41] genes as predictors of recurrence of lung cancers. The genes for which DNA methylation status at precancerous stages (β_N values) was associated with recurrence in the present study are different from the prognostic biomarkers selected in previous studies based on the DNA methylation status of tumorous tissues themselves.

In summary, DNA methylation status is not simply altered at precancerous stages, and is significantly correlated with recurrence after establishment of LADCs. DNA methylation alterations at precancerous stages are strengthened in comparison to normal lung tissues during progression to established LADC. DNA methylation profiles at precancerous stages may determine tumor aggressiveness through alterations in the expression of mRNAs for specific genes.

Supporting Information

Figure S1 Verification of the results of the Infinium assay using pyrosequencing methods. To overcome the PCR bias in pyrosequencing, the PCR conditions were optimized for each primer set, as described previously (Nagashio R, et al. Int J Cancer 129:1170, 2011). Pyrosequencing was performed for the *CNTNAP2, EVX1, GFRA1, PDE9A* and *TBX20* genes using 9 representative T samples and 9 corresponding N samples. β-values obtained from the Infinium assay were strongly correlated with DNA methylation levels obtained by pyrosequencing in all 5 genes, indicating that the results of the Infinium assay were successfully verified.
(TIF)

Figure S2 DNA methylation levels for the *ADCY5, EVX1, GFRA1, PDE9A* and *TBX20* genes in lung cancer cell lines. DNA methylation levels (β-values) for the *ADCY5, EVX1, GFRA1, PDE9A* and *TBX20* genes in all 4 of the lung cancer cell lines were examined by Infinium assay. To examine the effects of the DNA methylation inhibitor, 5-aza-2′-deoxycytidine, the top two cell lines showing the highest DNA methylation levels were selected for each gene: EBC-1 and A549 cells for the *ADCY5* gene, VMRC-LCD and EBC-1 cells for the *EVX1* gene, EBC-1 and PC9 cells for the *GFRA1* gene, VMRC-LCD and A549 cells for the *PDE9A* gene, and EBC-1 and PC9 cells for the *TBX20* gene.
(TIF)

Table S1 Characteristics of the lung cancer cell lines.
(PDF)

Table S2 Probe ID and primer sequences for quantitative real-time reverse transcription-PCR.
(PDF)

Table S3 The probes for which call proportions in all examined tissue samples were less than 90%.
(PDF)

Table S4 Multivariate analysis of clinicopathological parameters and mRNA expression levels of selected genes associated with recurrence in patients with lung adenocarcinomas.
(PDF)

Acknowledgments

The authors thank Y. Shimada for providing technical assistance.

Author Contributions

Conceived and designed the experiments: EA YK. Performed the experiments: TS EA TK. Analyzed the data: TS EA KS TB YK. Contributed reagents/materials/analysis tools: EA KT SW YK. Wrote the paper: TS EA YK.

References

1. Pao W, Girard N (2011) New driver mutations in non-small-cell lung cancer. Lancet Oncol 12: 175–180.
2. Greulich H (2010) The genomics of lung adenocarcinoma: opportunities for targeted therapies. Genes Cancer 1: 1200–1210.
3. Liu P, Morrison C, Wang L, Xiong D, Vedell P, et al. (2012) Identification of somatic mutations in non-small cell lung carcinomas using whole-exome sequencing. Carcinogenesis 33: 1270–1276.
4. Baylin SB, Jones PA (2011) A decade of exploring the cancer epigenome-biological and translational implications. Nat Rev Cancer 11: 726–734.
5. Kanai Y (2010) Genome-wide DNA methylation profiles in precancerous conditions and cancers. Cancer Sci 101: 36–45.
6. Kanai Y (2008) Alterations of DNA methylation and clinicopathological diversity of human cancers. Pathol Int 58: 544–558.
7. Kanai Y, Hirohashi S (2007) Alterations of DNA methylation associated with abnormalities of DNA methyltransferases in human cancers during transition from a precancerous to a malignant state. Carcinogenesis 28: 2434–2442.
8. Heller G, Zielinski CC, Zöchbauer-Müller S (2010) Lung cancer: from single-gene methylation to methylome profiling. Cancer Metastasis Rev 29: 95–107.
9. Hamilton JP (2011) Epigenetics: principles and practice. Dig Dis. 29: 130–135.
10. Eguchi K, Kanai Y, Kobayashi K, Hirohashi S (1997) DNA hypermethylation at the D17S5 locus in non-small cell lung cancers: its association with smoking history. Cancer Res 57: 4913–4915.
11. Zöchbauer-Müller S, Lam S, Toyooka S, Virmani AK, Toyooka KO, et al. (2003) Aberrant methylation of multiple genes in the upper aerodigestive tract epithelium of heavy smokers. Int J Cancer 107: 612–616.
12. Arai E, Chiku S, Mori T, Gotoh M, Nakagawa T, et al. (2012) Single-CpG-resolution methylome analysis identifies clinicopathologically aggressive CpG island methylator phenotype clear cell renal cell carcinomas. Carcinogenesis 33: 1487–1493.
13. Arai E, Ushijima S, Fujimoto H, Hosoda F, Shibata T, et al. (2009) Genome-wide DNA methylation profiles in both precancerous conditions and clear cell renal cell carcinomas are correlated with malignant potential and patient outcome. Carcinogenesis 30: 214–221.
14. Arai E, Kanai Y, Ushijima S, Fujimoto H, Mukai K, et al. (2006) Regional DNA hypermethylation and DNA methyltransferase (DNMT) 1 protein overexpression in both renal tumors and corresponding nontumorous renal tissues. Int J Cancer 119: 288–296.
15. Bibikova M, Le J, Barnes B, Saedinia-Melnyk S, Zhou L, et al. (2009) Genome-wide DNA methylation profiling using Infinium® assay. Epigenomics 1: 177–200.
16. Selamat SA, Chung BS, Girard L, Zhang W, Zhang Y, et al. (2012) Genome-scale analysis of DNA methylation in lung adenocarcinoma and integration with mRNA expression. Genome Res 22: 1197–1211.
17. Lockwood WW, Wilson IM, Coe BP, Chari R, Pikor LA, et al. (2012) Divergent genomic and epigenomic landscapes of lung cancer subtypes underscore the selection of different oncogenic pathways during tumor development. PLoS One 7: e37775.
18. Travis WD, Brambilla E, Müller-Hermelink HK, Harris CC (2004) World Health Organization Classification of Tumours. Pathology and Genetics of Tumours of the Lung, Pleura, Thymus and Heart. Lyon: IARC Press. pp. 35–44.
19. Sambrook J, Fritsch EF, Maniatis T (1989) Molecular Cloning. A Laboratory Manual (2nd ed). Cold spring Harbor: Cold Spring Harbor Laboratory Press. pp. E3–E4.
20. Yan L, Vatner DE, O'Connor JP, Ivessa A, Ge H, et al. (2007) Type 5 adenylyl cyclase disruption increases longevity and protects against stress. Cell 130: 247–258.
21. Okumura S, Vatner DE, Kurotani R, Bai Y, Gao S, et al. (2007) Disruption of type 5 adenylyl cyclase enhances desensitization of cyclic adenosine monophosphate signal and increases Akt signal with chronic catecholamine stress. Circulation 116: 1776–1783.
22. Poliak S, Salomon D, Elhanany H, Sabanay H, Kiernan B, et al. (2003) Juxtaparanodal clustering of Shaker-like K+ channels in myelinated axons depends on Caspr2 and TAG-1. J Cell Biol 162: 1149–1160.
23. Bralten LB, Gravendeel AM, Kloosterhof NK, Sacchetti A, Vrijenhoek T, et al. (2010) The CASPR2 cell adhesion molecule functions as a tumor suppressor gene in glioma. Oncogene 29: 6138–6148.
24. Briata P, Van De Werken R, Airoldi I, Ilengo C, Di Blas E, et al. (1995) Transcriptional repression by the human homeobox protein EVX1 in transfected mammalian cells. J Biol Chem 270: 27695–27701.
25. Ledda F, Paratcha G, Sandoval-Guzmán T, Ibáñez CF (2007) GDNF and GFRalpha1 promote formation of neuronal synapses by ligand-induced cell adhesion. Nat Neurosci 10: 293–300.
26. Fisher DA, Smith JF, Pillar JS, St Denis SH, Cheng JB (1998) Isolation and characterization of PDE9A, a novel human cGMP-specific phosphodiesterase. J Biol Chem 273: 15559–15564.
27. Saravani R, Karami-Tehrani F, Hashemi M, Aghaei M, Edalat R (2012) Inhibition of phosphodiesterase 9 induces cGMP accumulation and apoptosis in human breast cancer cell lines, MCF-7 and MDA-MB-468. Cell Prolif 45: 199–206.
28. Chakraborty S, Yutzey KE (2012) Tbx20 regulation of cardiac cell proliferation and lineage specialization during embryonic and fetal development in vivo. Dev Biol 363: 234–246.
29. Travis WD, Brambilla E, Noguchi M, Nicholson AG, Geisinger KR, et al. (2011) International association for the study of lung cancer/American thoracic society/European respiratory society international multidisciplinary classification of lung adenocarcinoma. J Thorac Oncol 6: 244–285.
30. Noguchi M, Morikawa A, Kawasaki M, Matsuno Y, Yamada T, et al. (1995) Small adenocarcinoma of the lung. Histologic characteristics and prognosis. Cancer 75: 2844–2852.
31. Kadara H, Kabbout M, Wistuba II (2012) Pulmonary adenocarcinoma: a renewed entity in 2011. Respirology 17: 50–65.
32. Kuang SQ, Tong WG, Yang H, Lin W, Lee MK, et al. (2008) Genome-wide identification of aberrantly methylated promoter associated CpG islands in acute lymphocytic leukemia. Leukemia 22: 1529–1538.
33. Tong WG, Wierda WG, Lin E, Kuang SQ, Bekele BN, et al. (2010) Genome-wide DNA methylation profiling of chronic lymphocytic leukemia allows identification of epigenetically repressed molecular pathways with clinical impact. Epigenetics 5: 499–508.
34. Omura N, Li CP, Li A, Hong SM, Walter K, et al. (2008) Genome-wide profiling of methylated promoters in pancreatic adenocarcinoma. Cancer Biol Ther 7: 1146–1156.
35. Truong M, Yang B, Wagner J, Kobayashi Y, Rajamanickam V, et al. (2012) Even-skipped homeobox 1 is frequently hypermethylated in prostate cancer and predicts PSA recurrence. Br J Cancer 107: 100–107.
36. Sinclair PB, Parker H, An Q, Rand V, Ensor H, et al. (2011) Analysis of a breakpoint cluster reveals insight into the mechanism of intrachromosomal amplification in a lymphoid malignancy. Hum Mol Genet 20: 2591–2602.
37. de Fraipont F, Levallet G, Creveuil C, Bergot E, Beau-Faller M, et al. (2012) An apoptosis methylation prognostic signature for early lung cancer in the IFCT-0002 trial. Clin Cancer Res 18: 2976–2986.
38. Dietrich D, Hasinger O, Liebenberg V, Field JK, Kristiansen G, et al. (2012) DNA methylation of the homeobox genes PITX2 and SHOX2 predicts outcome in non-small-cell lung cancer patients. Diagn Mol Pathol 21: 93–104.
39. Wu D, Xiong L, Wu S, Jiang M, Lian G, et al. (2012) TFPI-2 methylation predicts poor prognosis in non-small cell lung cancer. Lung Cancer 76: 106–111.
40. Verri C, Roz L, Conte D, Liloglou T, Livio A, et al. (2009) Fragile histidine triad gene inactivation in lung cancer: the European Early Lung Cancer project. Am J Respir Crit Care Med 179: 396–401.
41. Brock MV, Hooker CM, Ota-Machida E, Han Y, Guo M, et al. (2008) DNA methylation markers and early recurrence in stage I lung cancer. N Engl J Med 358: 1118–1128.
42. Morán A, Fernández-Marcelo T, Carro J, De Juan C, Pascua I, et al. (2012) Methylation profiling in non-small cell lung cancer: clinical implications. Int J Oncol 40: 739–746.
43. Carvalho RH, Haberle V, Hou J, van Gent T, Thongjuea S, et al. (2012) Genome-wide DNA methylation profiling of non-small cell lung carcinomas. Epigenetics Chromatin 5: 9.

Published OnlineFirst April 18, 2012; DOI:10.1158/1078-0432.CCR-12-0183

Clinical Cancer Research

Decreased Selenium-Binding Protein 1 Enhances Glutathione Peroxidase 1 Activity and Downregulates HIF-1 α to Promote Hepatocellular Carcinoma Invasiveness

Cheng Huang, Guangyu Ding, Chengyu Gu, et al.

Clin Cancer Res 2012;18:3042-3053. Published OnlineFirst April 18, 2012.

Published OnlineFirst April 18, 2012; DOI:10.1158/1078-0432.CCR-12-0183

Human Cancer Biology

Clinical Cancer Research

Decreased Selenium-Binding Protein 1 Enhances Glutathione Peroxidase 1 Activity and Downregulates HIF-1α to Promote Hepatocellular Carcinoma Invasiveness

Cheng Huang[1], Guangyu Ding[1], Chengyu Gu[1], Jian Zhou[1], Ming Kuang[3], Yuan Ji[2], Yifeng He[1], Tadashi Kondo[4], and Jia Fan[1]

Abstract

Purpose: We aimed to characterize the role of selenium-binding protein 1 (SBP1) in hepatocellular carcinoma (HCC) invasiveness and underlying clinical significance.

Experimental Design: SBP1 expression was measured in stepwise metastatic HCC cell lines by Western blotting. The role of SBP1 in HCC was investigated using siRNA. Immunofluorescence analyses were used to detect the interaction between SBP1 and glutathione peroxidase 1 (GPX1). Nineteen fresh tumor tissues and 323 paraffin-embedded samples were used to validate *in vitro* findings and to detect the prognostic significance of SBP1, respectively.

Results: Inhibition of SBP1 effectively increased cell motility, promoted cell proliferation, and inhibited apoptosis only under oxidative stress; it also greatly enhanced GPX1 activity without altering GPX1 expression and downregulated hypoxia-inducible factor-1α (HIF-1α) expression. SBP1 and GPX1 formed nuclear bodies and colocalized under oxidative stress. In freshly isolated clinical HCC tissues, decreased SBP1 was linked with increased GPX1 activity and correlated with vascular invasion. Tumor tissue microarrays indicated that SBP1 was an independent risk factor for overall survival and disease recurrence; patients with lower SBP1 expression experienced shorter overall survival periods and higher rates of disease recurrence ($P < 0.001$). Further analyses indicated that the predictive power of SBP1 was more significant for patients beyond the Milan criteria than patients within the Milan criteria.

Conclusions: Decreased expression of SBP1 could promote tumor invasiveness by increasing GPX1 activity and diminishing HIF-1α expression in HCC; SBP1 could be a novel biomarker for predicting prognosis and guiding personalized therapeutic strategies, especially in patients with advanced HCC. *Clin Cancer Res; 18(11); 3042–53. ©2012 AACR.*

Introduction

Selenium is an essential trace element with cancer-preventing activities that have been shown in many epidemiologic studies (1–3). The cellular biochemistry of selenium is a complex system that involves the expression of a wide range of selenium-containing proteins (4–6). Of these proteins, a 56-kDa molecule termed selenium-binding protein 1 (SBP1) was found to be the possible mediator of selenium's anticancer functions (7, 8). SBP1 is expressed in various cell types, including liver, heart, and kidney (2), and previous studies have established a solid connection between SBP1 and cancer. Decreased SBP1 was found in a vast number of human cancers, such as colorectal cancer (9), lung adenocarcinomas (10), ovarian cancer (11), gastric cancer (12), and hepatocellular carcinoma (HCC; ref. 13). However, the molecular mechanism underlying the tumor suppressive functions of SBP1 remains unclear.

Glutathione peroxidase 1 (GPX1) is also an important selenium-containing protein, in which selenium is a constituent of the amino acid selenocysteine. GPX1 is a ubiquitously expressed antioxidant enzyme that scavenges organic hydroperoxides and protects cells from reactive oxygen species (ROS) and hydrogen peroxide–induced or -dependent apoptotic injury (14, 15). Elevated GPX1 activity was reported to protect cancer cells from oxidative stress and anticancer agents (16–18). Previous studies using

Authors' Affiliations: [1]Liver Cancer Institute, [2]Department of Pathology, Zhongshan Hospital and Shanghai Medical School, Fudan University, Key Laboratory for Carcinogenesis & Cancer Invasion, the Chinese Ministry of Education, Shanghai; [3]Department of Hepatobiliary Surgery, The First Affiliated Hospital of Sun Yat-sen University, Guangzhou, PR China; and [4]Division of Pharmacoproteomics, National Cancer Center Research Institute, Tokyo, Japan

Note: Supplementary data for this article are available at Clinical Cancer Research Online (http://clincancerres.aacrjournals.org/).

C. Huang, G. Ding, and C. Gu contributed equally to this work.

Corresponding Authors: Jia Fan, Liver Cancer Institute, Fudan University, 136 Yi Xue Yuan Rd, Shanghai 200032, PR China. Phone: 0086-21-64037181; Fax: 0086-21-64037181; E-mail: fan.jia@zs-hospital.sh.cn and Tadashi Kondo, Division of Pharmacoproteomics, National Cancer Center Research Institute, 5-1-1 Tsukiji, Chuo-ku, Tokyo 104-0045, Japan. E-mail: proteomebioinformatics@gmail.com

doi: 10.1158/1078-0432.CCR-12-0183

Published OnlineFirst April 18, 2012; DOI:10.1158/1078-0432.CCR-12-0183

Translational Relevance

Selenium-binding protein 1 (SBP1) has been considered to be a protective agent against cancer. However, little is known about the function of SBP1 or its potential applications as a prognostic marker in hepatocellular carcinoma (HCC). Our findings indicate that SBP1 may act as a pro-oxidant rather than antioxidant through the interaction with glutathione peroxidase 1 and hypoxia-inducible factor-1α. Thus, the use of antioxidants such as glutathione in patients with HCC, especially patients with advanced-stage cancer, should be completed with caution. Furthermore, determination of SBP1 expression is especially useful for personalized therapeutic strategies and decisions about individuals beyond Milan criteria who could benefit from more aggressive treatment, such as chemotherapy or liver transplantation.

coimmunoprecipitation showed that these 2 distinct selenium-containing proteins (GPX1 and SBP1) can form a physical association that facilitates their interactions (19), but their possible roles in cancer development are still unknown. SBP1 is also known to have a hypoxia response element in its promoter region and to be a target gene of hypoxia-inducible factor-1α (HIF-1α; ref. 20), which is a fundamental mediator of cellular adaptation to microenvironmental stress, especially oxidative stress (21). The relationship between GPX1 and oxidative stress and the multifunctional role of HIF-1α in cancer biology may be associated with the antitumor activity of SBP1.

HCC is the sixth most common malignancy and the third leading cause of cancer death worldwide (22). Although early diagnosis and surgical treatments have significantly improved overall patient outcomes, long-term survival is still low due to high rates of recurrence and metastasis. Resistance toward cytotoxic chemotherapy also affects survival and prognosis in patients with HCC (23). We and other groups have found that the expression of SBP1 is decreased in most HCCs and is associated with poor outcomes (13), but the possible molecular mechanism of SBP1 in HCC biology, particularly in cancer invasion and metastasis, has not been studied. Given the relationship among SBP1, GPX1, HIF-1α, and oxidative stress in the HCC microenvironment, in this study, we aimed to explore the role of SBP1 in cancer invasion and metastasis. We found that decreased SBP1 could promote HCC invasion/metastasis and lead to poor prognosis through the enhancement of GPX1 activity and the downregulation of HIF-1α.

Materials and Methods

Cell lines

The normal liver cell line L-02 and the HCC cell lines HepG2, Hep3B, SMMC7721, Huh 7, and PLC/PRF/5 were purchased from the Institute of Biochemistry and Cell Biology, Chinese Academy of Sciences (CAS). HCC cell lines with stepwise metastatic potential (MHCC97L, MHCC97H, HCCLM3, and HCCLM6, which are HBV-positive cell lines with the same genetic background but different lung metastatic potentials) were established at our institute (24, 25). Cell lines were grown in Dulbecco's Modified Eagle's Medium (DMEM) or RPMI-1640 (Invitrogen/GIBCO) supplemented with 10% FBS (Invitrogen/GIBCO) at 37°C in 5% carbon dioxide.

We used hydrogen peroxide (Sigma) as ROS resources to simulate oxidative stress *in vitro*. A concentration of 300, 100, and 50 μmol/L was used in the apoptosis assay, proliferative assay, and immunofluorescence assay, respectively.

Patients and samples

Patients with HCC ($n = 342$) who underwent surgical treatment at the Zhongshan Hospital at Fudan University (Shanghai, China) were enrolled in this study. Patients were divided into 2 cohorts according to their dates of surgery. To ensure accurate analysis of GPX1 activity, tumor tissue samples were freshly isolated from 19 patients during a 2-week period in 2011 (cohort 1). Tumor specimens used in tissue microarrays (TMA) analyses were consecutively chosen from 323 patients with HCC between 2003 and 2004 (cohort 2). Ethical approval for human subjects was obtained from the Institutional Review Board, and written informed consent was obtained from the patients.

Patients in cohort 1 were classified into 2 groups according to the extent of vascular invasion detected. Patients in cohort 2 were followed up every 2 months during the first postoperative year and at least every 3 to 4 months thereafter until March 15, 2009, 9 of the 323 patients were lost. The median follow-up period was 60 months (range, 2–85 months). Overall survival (OS) was defined as the interval between surgery and death or between surgery and the last observation point. Time to recurrence was defined as the interval between the date of surgery and the date of diagnosis of intrahepatic recurrence and metastasis. Using 24 months as the cutoff value, all cases of recurrence were divided into early recurrence ($n = 147$) or late recurrence ($n = 55$; ref. 26). Preparations of tissue samples are described in the Supplementary Appendix.

Molecular and cell biology assays

Western blotting, quantitative real-time PCR (qRT-PCR), migration analysis, proliferation analysis, apoptosis assay, and immunofluorescence assay were conducted as described previously (27). Detailed information is provided in the Supplementary Appendix.

RNA interference

For siRNA-mediated SBP1 silencing, the following target siRNA sequences were used: sense, CUUGGAGGCACCAAGAAAUTT and antisense, AUUUCUUGGUGCCUCCAAGTT. The RNA duplexes were synthesized by the Genepharma Company. Transfection of the siRNAs into the SMMC7721 cell line was carried out with Lipofectamine 2000 (Invitrogen) according to the manufacturer's instructions.

Published OnlineFirst April 18, 2012; DOI:10.1158/1078-0432.CCR-12-0183

Measurement of GPX1 activity

Measurement of GPX1 activity was conducted as described previously (28). Detailed information is provided in the Supplementary Appendix.

TMAs and immunohistochemistry

TMAs were constructed by the Shanghai Biochip Co., Ltd. The primary antibody used in immunohistochemistry was SBP1 (1:500; MBL). Immunohistochemistry was carried out using a 2-step protocol (Novolink Polymer Detection System; Novocastra). Negative control slides in which the primary antibodies were omitted were included in all assays.

To validate concordance between TMAs and whole tumor sections, we further detected the expression of SBP1 by immunohistochemistry in 50 corresponding whole tumor sections randomly chosen from the 323 cases.

Evaluation of immunohistochemical variables

Immunohistochemical scores were assessed by 2 independent pathologists without knowledge of patient characteristics, and the scores for all cases were compared with check for discrepancies. The final scores were assigned by discussion. Scores were assigned as intensity and percentage of positively staining tumor cell cytoplasm and nuclei in the whole tissue sample. Specifically, the immunostains were scored using a 4-point scale (0–+++) system based on the number of positive cells and the intensity of staining.

Correlations of SBP1 expression profiles with clinical demographics, OS, and recurrence rates were evaluated. Further details about these methods are described in the Supplementary Appendix.

Statistical analysis

The software package SPSS v13.0 (SPSS Inc.) was used for statistical analyses. Univariate and multivariate Cox proportional hazards models were used to identify relevant prognostic factors. Kaplan–Meier survival curves and the log-rank (Mantel–Cox) test were used to compare patient survival and recurrence probability between subgroups (26). All statistical tests were 2-sided, and a P value less than 0.05 was considered statistically significant.

Results

SBP1 is minimally expressed in most human HCC cell lines and inhibits cell migration

We detected the expression levels of SBP1 in current HCC cell lines (Fig. 1A). SBP1 was highly expressed in normal liver cells whereas barely detected in the highly metastatic HCC cell lines (MHCC97L, MHCC97H, HCCLM3, and HCCLM6). HCC cell lines with low metastatic potential also expressed marginal levels of SBP1 with the exception of SMMC7721. SMMC7721 was the only HCC cell line that expressed a high level SBP1, and we chose this cell line for further study. The expression of SBP1 in SMMC7721 72 hours after siRNA transfection was downregulated to a minimal level (Fig. 1B and D) compared with SBP1 expression in the negative control.

Cell migration of SBP1-silenced SMMC7721 cells and negative control cells was assessed via Transwell chambers (Fig. 1C) and wound-healing assays (Fig. 1E). The results showed significant differences indicating that SBP1 greatly inhibits cancer cell migration.

SBP1 inhibits proliferation and induces apoptosis only after hydrogen peroxide treatment

We used the CCK-8 assay to determine whether SBP1 might interfere with cell proliferation and we observed that SBP1 only inhibited cellular proliferation following hydrogen peroxide treatment (Fig. 2A). When cells were cultured in normal medium, SBP1 did not inhibit cell proliferation, and the proliferation rate of the control group was slightly higher than that of the SBP1-silenced group. However, if 100 μmol/L of hydrogen peroxide was added to the culture medium, SBP1 greatly inhibited cell proliferation. The inhibition of proliferation began 24 hours following treatment, and the cell counts of the control group were slightly decreased at 48 and 72 hours whereas the SBP1-silenced group cells were unaffected in the presence of hydrogen peroxide. These results indicated that SBP1 alone could not inhibit cell proliferation.

The apoptosis assay showed results similar to those obtained earlier (Fig. 2B). No significant differences in apoptosis rates were observed between the 2 groups if given normal culture medium. However, if 300 μmol/L of hydrogen peroxide was added and cells were incubated for 24 hours, the apoptosis rate of the SBP1-silenced group was dramatically reduced compared with that of the negative control group, indicating that SBP1 could somehow facilitate the hydrogen peroxide–induced apoptosis.

SBP1 and HIF-1α interactions

Figure 2C showed the interactions of SBP1, HIF-1α, and GPX1 expressions under different conditions. The hydrogen peroxide–treated groups were treated with 50 μmol/L hydrogen peroxide for 24 hours before protein extraction. The expression of HIF-1α was increased by hydrogen peroxide treatment, as shown by the control groups (SMMC7721 and SMMC7721-Mock), and an increase in SBP1 expressions could also be observed in the same groups. This is consistent with the finding that SBP1 is a target gene for HIF-1α (20). However, in the SMMC7721 groups where SBP1 expression was downregulated by siRNA treatment, the expression of HIF-1α was not elevated by hydrogen peroxide treatment. This might indicate that SBP1 could also somehow counter-regulate the expression of HIF-1α following hydrogen peroxide treatment.

The expression of GPX1, however, was not associated with either SBP1 or HIF-1α (Fig. 2C), although a slight increase could be detected following treatment with hydrogen peroxide.

SBP1 greatly inhibits GPX1 activity, not expression level *in vitro*

We measured the activities of GPX1 under different conditions *in vitro* (Fig. 2D). Compared with the control

Published OnlineFirst April 18, 2012; DOI:10.1158/1078-0432.CCR-12-0183

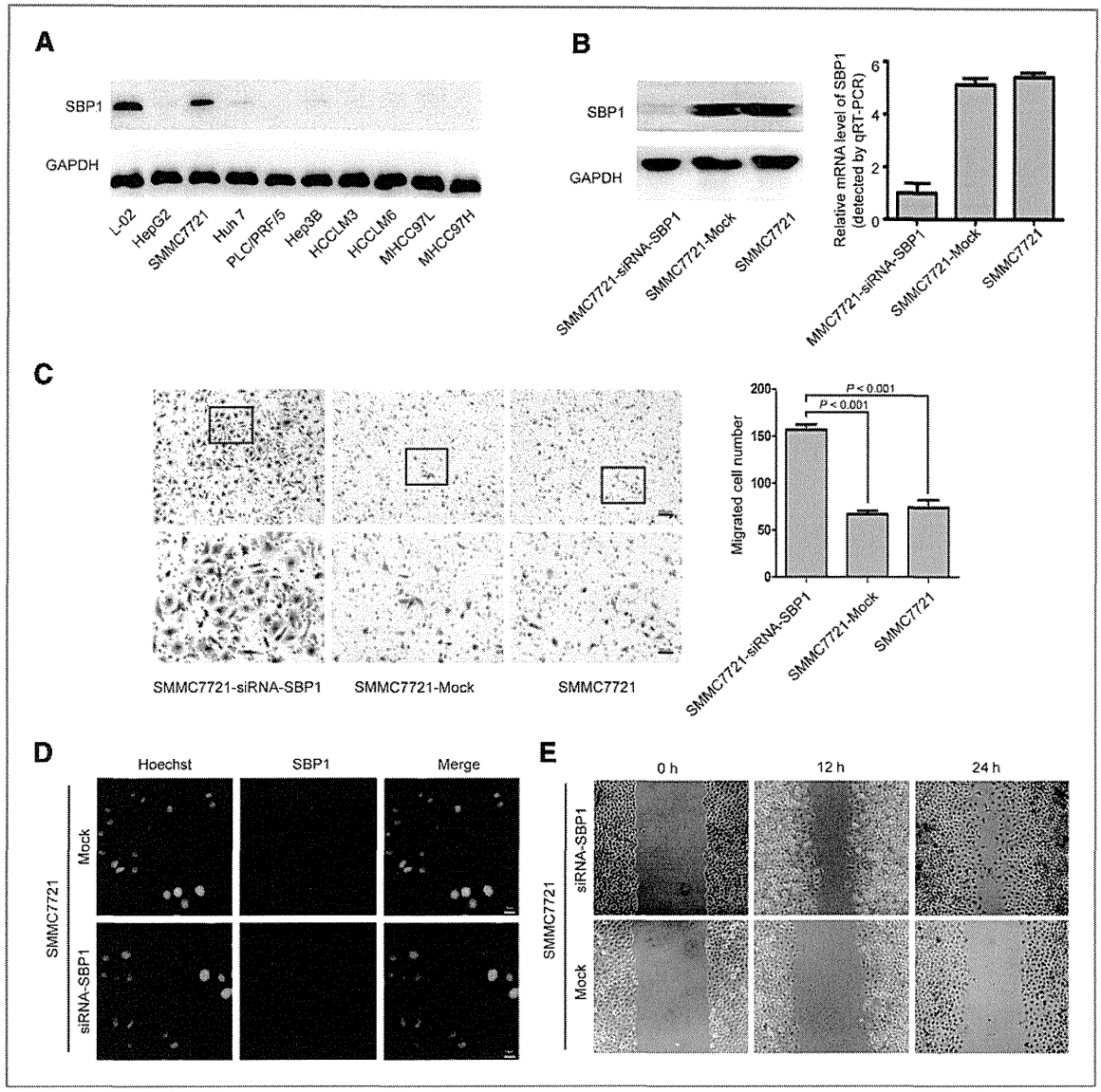

Figure 1. Expression of SBP1 in HCC cell lines and migration analysis of SBP1 by siRNA. A, Western blot analysis of SBP1 expression in cell lines L-02, HepG2, SMMC7721, Huh7, PLC/PRF/5, Hep3B, HCCLM3, HCCLM6, MHCC97L, and MHCC97H. L-02 and SMMC7721 both expressed relatively high levels of SBP1 compared with other HCC cell lines. Glyceraldehyde-3-phosphate dehydrogenase (GAPDH) was used as a loading control. B, both Western blotting and qRT-PCR results showed that SBP1 expression in SMMC7721 cells was downregulated to a marginal level by siRNA treatment. Total protein and RNA were extracted from the cells 72 hours after transfection. C, Transwell assays showed that the number of migrated cells in the SBP1-siRNA group increased significantly compared with those in the control group. Representative data of 3 independent experiments are shown. D, immunofluorescence showed the location of SBP1 in SMMC7721-Mock and SMMC7721-siRNA samples. E, the wounds were nearly closed 24 hours after scratch in the SBP1-siRNA group compared with the control group. All experiments were repeated at least 3 times.

groups, the GPX1 activities in the SBP1-silenced groups had increased by 4- or 5-fold. This dramatic increase in GPX1 activity indicates that SBP1 may greatly inhibit GPX1 activity. Given the fact that the expression levels of GPX1 in different groups were unchanged (Fig. 2C), SBP1 might inhibits GPX1 through a post-translational way.

SBP1 and GPX1 formed special bodies and colocalized in the nuclei following hydrogen peroxide treatment

Under normal conditions, GPX1 localized exclusively in the cytoplasm but SBP1 could be found both in the cytoplasm and the nucleus (Fig. 3A). However, when cells were treated with hydrogen peroxide, we observed that both GPX1 and SBP1 had established specific nuclear bodies,